The ionospheric response to interplanetary magnetic field variations: Evidence for rapid global change and the role of preconditioning in the magnetosphere

Masakazu Watanabe,[1] Natsuo Sato,[1] Raymond A. Greenwald,[2] Michael Pinnock,[3] Marc R. Hairston,[4] Richard L. Rairden,[5] and Don J. McEwen[6]

Abstract. We have found observational evidence for a rapid communication of interplanetary magnetic field (IMF) changes to the global ionosphere and evidence for the state of the magnetosphere in the previous hour conditioning this response. These conclusions are drawn from a case study of sunward flow bursts on the nightside polar cap boundary observed by geomagnetically conjugate HF radars. The flow burst excitation consists of two factors: (1) At the time of the flow burst, the magnetosphere still held a memory of the stable and northward IMF period that had persisted up until 1 hour before the flow burst (internal condition). During the northward IMF period a theta aurora associated with a sunward flow channel was formed in the polar cap. After that the IMF turned southward, and the transpolar arc decayed antisunward. However, by the time of the flow burst (i.e., 1 hour after the IMF southward turning), the Sun-aligned arc had not yet completely vanished, and in the poleward expanded portion of the northern plasma sheet, there was still a remnant of the sunward flow channel susceptive to an external forcing. (2) One hour after the southward turning of the IMF a sharp IMF transition from southward to northward B_Z impinged on the dayside magnetopause (external condition). On arriving at the dayside cusp ionosphere the B_Z transition signal pervaded the entire polar cap ionosphere instantaneously (<1 min) and reached the nightside plasma sheet. There, the remnant of the sunward flow channel was reactivated by the B_Z transition, and a sunward flow burst was observed first in the northern ionosphere and then in the southern ionosphere with a 7-min time delay. Thus the sunward flow burst represents a rapid global response of the ionosphere starting 2–3 min after the IMF change at the subsolar magnetopause.

1. Introduction

An important consequence of the plasma processes occurring at the magnetopause boundary and in the magnetotail is the excitation of convective flow in the polar ionosphere. Up until the mid-1980s, ionospheric plasma flow had been studied primarily using low-altitude polar-orbiting satellites to obtain statistical or synthesized convection patterns assuming steady state convection [e.g., *Heppner and Maynard*, 1987]. The major success of these studies was the identification that the convection pattern was strongly dependent on the direction of the interplanetary magnetic field (IMF), showing that magnetic reconnection was the main driving force of the plasma flow in the magnetosphere-ionosphere system. The statistical convection pattern thus determined, however, does not include any information on the time-dependent effects; that is, the manner in which the convection pattern energizes or reconfigures in response to the changes of the IMF is not determined. From the late 1980s onward the dynamical feature of the time-dependent flow has been the focus of much research effort, and a number of studies have been undertaken to describe the ionospheric response to changing IMF. For example, the response to a northward turning of the IMF has been investigated by *Clauer and Friis-Christensen* [1988], *Knipp et al.* [1991], *Ridley et al.* [1998], and *Taylor et al.* [1998]. All these studies were performed using ionospheric radar and ground magnetometer data. The time-dependent ionospheric convection is not amenable to investigation using spacecraft data [e.g., *Hairston and Heelis*, 1995] but is accessible to ground-based data.

The present paper deals with radar observations of transient ionospheric phenomena associated with IMF changes. Our study was originally motivated by our finding of sunward flow bursts on the nightside polar cap boundary using HF radar data. It is now established that ionospheric convection is driven primarily by magnetic reconnection at the dayside magnetopause and in the magnetotail. In the ionosphere the consequence of magnetic reconnection is expected to appear as bursts or enhancements of plasma flow [e.g., *Cowley and Lockwood*, 1992]. The magnetotail reconnection always produces antisunward flows in the nightside ionosphere. In fact, antisunward flow bursts on the nightside are not rare, and some of

[1]National Institute of Polar Research, Tokyo.
[2]Applied Physics Laboratory, Johns Hopkins University, Laurel, Maryland.
[3]British Antarctic Survey, Natural Environment Research Council, Cambridge, England.
[4]William B. Hanson Center for Space Sciences, University of Texas at Dallas, Richardson.
[5]Space Sciences Laboratory, Lockheed Missiles and Space Company, Inc., Palo Alto, California.
[6]Department of Physics and Engineering Physics, College of Arts and Science, University of Saskatchewan, Saskatoon, Canada.

them are well interpreted by reconnection in the magnetotail [*Watanabe et al.*, 1998]. However, sunward flows on the nightside polar cap boundary cannot be attributable to magnetotail reconnection. Furthermore, there exist no good candidates in the magnetotail for driving the sunward flow in the ionosphere. Thus the sunward flow burst we describe is not a typical feature of the magnetosphere-ionosphere system. To our knowledge, there has been no prior report of bursty sunward flows in the nightside polar ionosphere.

As mentioned above, flows stimulated by magnetotail reconnection are always antisunward in the nightside ionosphere, so we need to seek another driving force for these sunward flow bursts. It is known that in the daytime sector the convection can show a reverse pattern (i.e., sunward flows at high latitudes) for northward IMF [e.g., *Heppner and Maynard*, 1987]. It is therefore natural to suspect that a northward IMF can stimulate sunward flows on the nightside. This was, in fact, the case for the sunward flow bursts examined in this paper. As we will show, the sunward flow bursts were triggered by a positive IMF B_Z transition that impinged on the dayside magnetopause. The IMF B_Z change, however, was not the only factor that stimulated the flow bursts. At the time of the IMF transition the magnetosphere was in a state that was susceptible to producing such bursts. Up until 1 hour before the IMF B_Z transition, the IMF was stable and due northward for ~1.5 hours with a theta aurora in the polar cap. After that, the IMF turned southward, but a remnant of the transpolar arc persisted after the southward turning of the IMF and remained until the IMF again turned northward. Thus one important aspect in the sunward flow burst event is the history of the magnetosphere before the IMF B_Z transition. In this paper we examine in detail the morphology of the magnetosphere and the ionosphere during the intermediate southward IMF state using coordinated space-borne and ground-based observations in the key regions.

We also discuss the nature of the global magnetosphere-ionosphere response to the IMF B_Z transition and its timescales. This is a topic of recent controversy [*Lockwood and Cowley*, 1999; *Ridley et al.*, 1999]. Some results reported in the literature suggest that the ionospheric convection change induced by the dayside reconnection rate variation (i.e., IMF B_Z changes) starts first in the midday sector and then propagates eastward and westward with speeds of 2–5 km s^{-1}. Therefore there is a significant (5–10 min) time delay between the dayside and dawn/duskside responses [*Lockwood et al.*, 1986; *Etemadi et al.*, 1988; *Todd et al.*, 1988; *Saunders et al.*, 1992; *Taylor et al.*, 1998]. In contrast to this propagating structure picture, some authors argue that the global ionospheric response is much faster and that the electric field of the IMF is communicated to the entire polar cap ionosphere in less than 1 min. *Ruohoniemi and Greenwald* [1998] investigated the electric field response of the ionosphere to a sharp (<2 min) southward turning of the IMF using Super Dual Auroral Radar Network (SuperDARN) data distributed in a wide range of magnetic local times (1200–2200); they found that sharp changes of ionospheric flow were observed everywhere simultaneously (within 2 min temporal resolution). *Ridley et al.* [1997, 1998], using the Assimilative Mapping of Ionospheric Electrodynamics (AMIE) technique, investigated the global ionospheric response to IMF changes by examining polar cap potentials subtracted from a base potential pattern. They found that the residual potential pattern does not show antisunward motion (i.e., stationary in its location and shape) but instead the strength of the convection (i.e.,

the magnitude of the voltage) increases or decreases with time. The work by *Ridley et al.* [1998] was commented on by *Lockwood and Cowley* [1999]. Ridley et al.'s interpretation indicates that at the onset of the dayside convection change, the nightside flux tubes simultaneously start to move in the ionosphere while in the magnetosphere they are stationary. Lockwood and Cowley commented that there was no reason for this to happen.

In the context of this controversy the event in this paper offers good material for the discussion on the global response of the magnetosphere-ionosphere system. The morphology supports very quick ionospheric response, without significant delay between the dayside and nightside. At the same time, the morphology also suggests that the fast response is not associated with the onset of the nightside plasma sheet reconfiguration. These facts imply that we are seeing two different responses of the nightside magnetosphere-ionosphere system. In section 6.3 we discuss the two different responses on the basis of the observations. In this event the sunward flow burst was simultaneously observed in the geomagnetically conjugate regions in the Northern and Southern Hemispheres. Although the main part of the discussion is based on the Northern Hemisphere data, the geomagnetically conjugate observations, supporting each other, provide us with a firm basis for the comprehensive interpretation. Thus, in sections 3–5, we present both the Northern and Southern Hemisphere data in parallel for the assimilative and correlative study of the global magnetosphere-ionosphere system.

2. Background

The sunward flow burst event to be presented here occurred on February 2, 1995. During the preliminary stage of this study, we found that the HF radar at Goose Bay (described in the appendix) occasionally observes unusual sunward flows at high (>70° magnetic) latitudes in the premidnight sector, with a relatively high (>500 m s^{-1}) speed persisting for more than 10 min. On the nightside the flow driven by magnetotail reconnection is always antisunward in the ionosphere [e.g., *Cowley and Lockwood*, 1992], and in fact, observed convection patterns normally show antisunward flow [e.g., *Heppner and Maynard*, 1987]. Thus sunward flow on the nightside is a rare occurrence. From a survey of Goose Bay data during three boreal winters for 1994–1997, we found 10 such sunward flow events. These 10 events are found to occur preferably during periods of low K_p and positive IMF B_Z, giving the impression that they are associated with theta auroras. The theta aurora is an auroral configuration found preferably for northward IMF and characterized by a ring of luminosity termed the auroral oval and a "bar" across the polar cap from noon to midnight; the transpolar arc or the theta bar is suggested to occur on closed field lines connected to the plasma sheet, and the plasma convection associated with the transpolar arc is observed to be primarily sunward [e.g., *Frank et al.*, 1986]. We thus suspected that the observed sunward flow was responsible for the theta aurora. In fact, in three of the three events in which ground optical data were available, Sun-aligned transpolar arcs were identified in the polar cap during or near the sunward flow interval. However, the IMF variations during and preceding the sunward flow period were, in general, too complicated to elucidate the cause and effect of the phenomenon. The only exception was the February 2, 1995, event we demonstrate here. On this day the IMF variations were somewhat simple (though not too simple), which enabled us to identify
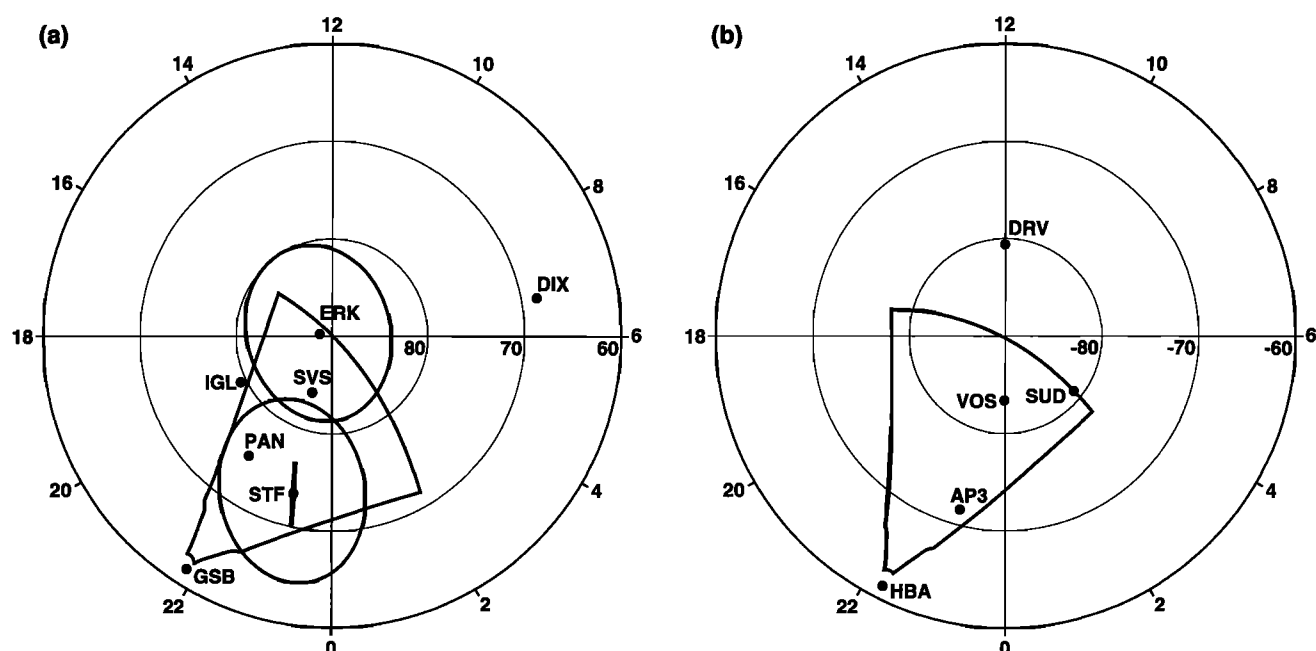
Figure 1. The configurations of ground observations at 0130 UT February 2, 1995, for (a) north and (b) south. Fans are the fields of view of the HF radars at Goose Bay (GSB) (Plate 1) and Halley (HBA) (Plate 3). Ellipses show the fields of view of the all-sky cameras at Eureka (ERK) (Plate 5) and Søndre Strømfjord (STF) (Plate 2). The thick curve passing through STF is the scanning direction of the Sondrestrom incoherent scatter (IS) radar (Figure 5). Geomagnetic observatories in Figure 3 are also shown by solid circles: Dixon (DIX), Eureka (ERK), Savissivik (SVS), Igloolik (IGL), Pangnirtung (PAN), Dumont d'Urville (DRV), Sude (SUD), Vostok (VOS), and Automatic Geophysical Observatory (AGO) P3 (AP3) (see also Table 1).

the origin of the sunward flow. In addition, other instruments in the key regions, both on the ground and in space, were working very effectively on this day. For these reasons we have selected this event for the case study.

3. An Overview of the Data Set

On February 2, 1995, many instruments in the key regions were operational. In this paper we utilized the HF radars at Goose Bay (Plate 1) and Halley (Plate 3), the all-sky cameras at Eureka (Plate 5) and Søndre Strømfjord (Plate 2), the incoherent scatter radar at Søndre Strømfjord (the Sondrestrom incoherent scatter (IS) radar) (Figure 5), a number of Defense

Meteorological Satellite Program (DMSP) and National Oceanic and Atmospheric Administration (NOAA) satellite overflights (Figure 4 and Plate 4), and a worldwide network of ground magnetometers (Figure 3). Data from instruments will be discussed in sections 4 and 5. A brief description of the instruments, with introductions to the images and maps, is given in the appendix. Here we survey the observational items for the parallel discussion of the multi-instrument data in sections 4 and 5.

Figure 1 shows the configurations of ground observations at 0130 UT February 2, 1995, in geomagnetic latitude and local time coordinates. Locations of key ground observatories are listed in Table 1. Throughout this paper, magnetic latitude

Table 1. Locations of Radars and Geomagnetic Observatories[a]

	Geographic Latitude, °N	Geographic Longitude, °E	AACGM Latitude, °N	AACGM Longitude, °E
Goose Bay (GSB) (Canada)	53.3	−60.5	61.7	23.2
Halley (HBA) (Antarctica)	−75.5	−26.6	−61.3	29.0
Søndre Strømfjord (STF) (Greenland)	67.0	−51.0	73.3	41.7
Dixon (DIX) (Russia)	73.5	80.6	68.4	156.0
Eureka (ERK) (Canada)	80.0	−85.9	88.7	−44.4
Savissivik (SVS) (Greenland)	76.0	−65.1	83.9	36.1
Igloolik (IGL) (Canada)	69.3	−81.8	79.4	−8.1
Pangnirtung (PAN) (Canada)	66.1	−65.8	75.0	20.4
Dumont d'Urville (DRV) (Antarctica)	−66.7	140.0	−80.6	−124.2
Sude (SUD) (Antarctica)	−71.3	96.7	−81.0	107.3
Vostok (VOS) (Antarctica)	−78.5	106.8	−83.4	54.7
AGO P3 (AP3) (Antarctica)	−82.8	28.6	−71.6	40.7

[a]AACGM, Altitude Adjusted Corrected Geomagnetic coordinates; AGO, Automatic Geophysical Observatory.

(MLAT) and magnetic longitude (MLON) are expressed in the Altitude Adjusted Corrected Geomagnetic (AACGM) coordinates system [Bhavnani and Hein, 1994] based on the International Geomagnetic Reference Field Epoch 1995. The fans in Figures 1a and 1b show the fields of view of the Goose Bay (GSB) and Halley (HBA) HF radars, respectively. Two-dimensional line-of-sight Doppler velocities from the HF radars are used to determine the electric field response of the ionosphere to IMF changes. The ellipses in Figure 1a show the fields of view of the all-sky cameras at Eureka (ERK) and Søndre Strømfjord (STF). Optical data from the two cameras are used to observe the evolution of the theta aurora (transpolar arcs) and to infer the magnetotail structure. In particular, the 630-nm emission data from STF are used to determine the motion of the nightside polar cap boundary. The thick curve passing through STF shows the scanning direction of the Sondrestrom IS radar. Ion drift velocities in this direction are used to supplement the Goose Bay HF radar data. In addition to the ground instruments, we use precipitating particle and ion drift data obtained by polar-orbiting DMSP F10/ F11/F12 and NOAA 12 satellites at an altitude of 840 km, to monitor the polar cap evolution globally.

Here we remark on the terminology in this paper in order to avoid confusion. From now on, we use "poleward/equatorward" and "sunward/antisunward" interchangeably. In general, poleward/equatorward are preferably used for images presented in the Earth-reference frame (e.g., the radars and the STF all-sky camera), but sunward/antisunward are also used in the same meaning. As is evident from Figure 1, during the UT interval of our interest, poleward and equatorward correspond to sunward and antisunward, respectively, in the Sun-reference frame.

4. Sunward Flow Bursts Triggered by an IMF B_Z Transition

4.1. Interplanetary Disturbances

Figures 2a–2f show plasma and magnetic field data obtained by the Wind spacecraft for 2100 UT, February 1, 1995, to 0300 UT, February 2, 1995. Wind was located at $(X, Y, Z) \approx (187, -50, -33)$ R_E (R_E being the radius of the Earth) in Geocentric Solar Magnetospheric (GSM) coordinates and was monitoring the near-Earth interplanetary physical parameters. Figures 2a–2c show solar wind bulk velocities, densities, and thermal velocities, respectively. From these plasma parameters it is clear that the solar wind dynamic pressure is nearly constant during this time interval. Figures 2d–2f show the IMF B_X, B_Y, and B_Z components, respectively, in GSM coordinates. A noteworthy feature in the IMF variations is that the IMF is stably northward with $B_Z \approx +6$ nT for ~3 hours prior to 0011 UT, February 2, except for the transient negative excursion centered around 2207 UT, February 1. After 0011 UT, B_Z becomes negative and then positive once again for 0102–0114 UT.

During this time interval the Geotail spacecraft traversed the subsolar magnetosheath from dawnside $((X, Y, Z) \approx (10, -2, 0)$ $R_E)$ to duskside ($\sim(11, 7, 3)$ R_E in GSM coordinates), and it monitored the magnetosheath magnetic field (MMF) upstream of the dayside magnetopause. Figure 2j shows the root-mean-square (RMS) of the magnetic field observed by Geotail. From the energy-versus-time spectrograms of low-energy (<40 keV) ions and electrons (not shown here),

we know that Geotail left the magnetosphere and entered into the magnetosheath at ~2107 UT, February 1. This is also clearly identified in the RMS profile, exhibiting an abrupt jump at that time from lower to higher values. After that, Geotail was in the magnetosheath continuously. Figures 2g–2i show the MMF B_X, B_Y, and B_Z components, respectively, observed by Geotail in GSM coordinates. The magnitude of B_X is much smaller than that of the other two components. Above all, B_X for 2244–0022 UT is constantly near zero. This would be because of the draping effect near the subsolar magnetosheath. The overall trends in B_Y and B_Z variations are similar to those of Wind. However, we notice that dissimilarities do exist, in particular, after 0020 UT, February 2. Three-dimensional structure of the solar wind would be a possible cause of the discrepancy, although details are unknown. In this paper we use the subsolar MMF observed by Geotail as the monitor of the IMF variations that affect the magnetosphere. Since we cannot find any disturbances in the solar wind dynamic pressure, it would be reasonable to examine the cause of ionospheric disturbances in terms of the IMF variations.

4.2. Sunward Flow Bursts on the Nightside Polar Cap Boundary

Plates 1d–1l demonstrate a time sequence of Doppler velocities observed by the Goose Bay radar for 0125:47–0140:45 UT, February 2, 1995. The magnetic local time (MLT) of a specific point is given approximately by MLT = MLON/15 + UT + 18.8, so the radar field of view (~10°–50° MLON) during this time interval covers the ~2100–2340 MLT sector (see Figure 1a). Blue represents velocities toward the radar (positive values), whereas red represents velocities away from the radar (negative values). In this paper we discuss exclusively the line-of-sight velocities. The Stokkseyri radar in Iceland, which measures the east-west component in the Goose Bay radar field of view, received no good echoes from the common viewing area of the two radars, so we cannot discuss two-dimensional vector velocities. However, at high (>70°) latitudes in the premidnight sector the plasma flow is dominated by the north-south component, and the line-of-sight component in Plate 1 is sufficient for the discussion here unless we examine quantitatively the magnitude of the flow speed. In contrast, at auroral zone latitudes (MLAT < 70°) the plasma flow becomes oval-aligned, and the east-west component becomes important. The time sequence of Plates 1d–1l shows that the line-of-sight velocities at 65°–70° MLAT are constantly toward in the eastern part and away in the western part of the field of view. If we assume the flow is uniform along parallels of latitude, this line-of-sight velocity pattern indicates a presence of westward flow [e.g., Freeman et al., 1991]. Namely, Goose Bay is in the eveningside convection cell.

In Plates 1i–1k we can discern a region of poleward flows in the middle of the field of view (~75°–80° MLAT and ~15°–35° MLON, as indicated by yellow arrows), surrounded by regions of equatorward flows. The flow speed exceeds 600 m s^{-1} at its peak (yellow regions). This poleward (i.e., sunward) flow is the subject of our present study. This sunward flow is traceable back to the scan of Plate 1e; in the preceding scan (Plate 1d) we cannot identify the sunward flow region, although radar echoes are somewhat poor. Thus the sunward flow region emerges at ~0128 UT (Plate 1e), and its center shifts somewhat equatorward in the subsequent scan (Plate 1f). It starts to enhance at ~0133 UT (Plate 1h) and attains its peak at ~0137 UT (Plate 1j). Then it starts to decay at ~0139 UT (Plate 1l)
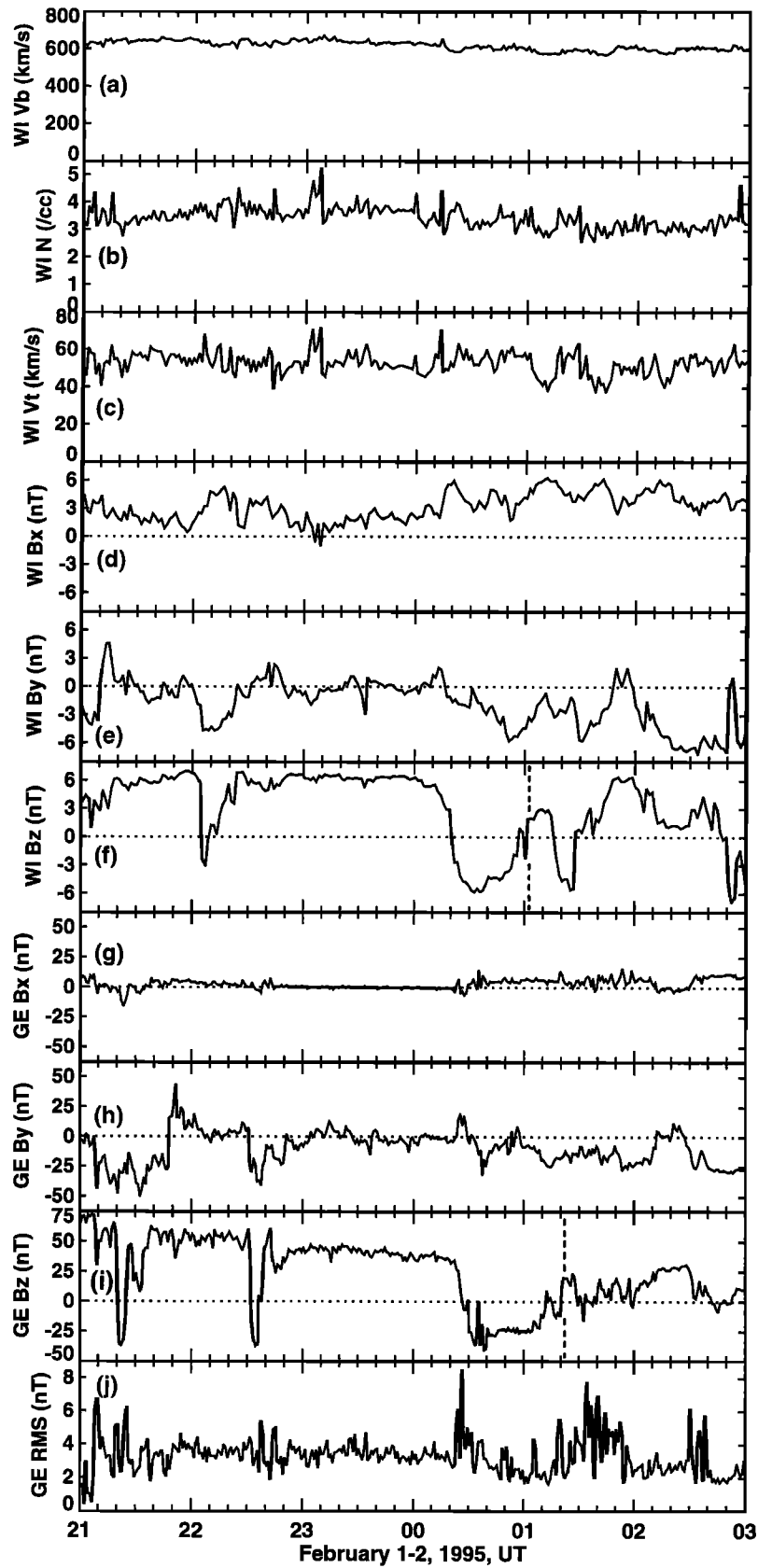
Figure 2. Observations by Wind at $(X, Y, Z) \approx (187, -50, -33)$ R_E: (a–c) the bulk speed (V_b), density (N), and thermal speed (V_t) of the solar wind and (d–f) the B_X, B_Y, and B_Z components (in GSM coordinates) of the IMF. Observations by Geotail in the subsolar magnetosheath at $X \approx 11$ R_E: (g–i) the B_X, B_Y, and B_Z components (in GSM coordinates) and (j) the root-mean-square (RMS) of the magnetosheath magnetic field (MMF).

but survives until ~0141 UT (the subsequent scan of Plate 1l is not shown here). Thus the sunward flow lasted ~13 min (0128–0141 UT).

Plates 2f–2t show a time sequence of Søndre Strømfjord all-sky images (630-nm emission) including the sunward flow burst period. In Plates 2m–2t we see an east-west arc migrating equatorward in the middle of the field of view. This arc is traceable back to 0120 UT (Plate 2f), where the arc enters the field of view in the north, elongated in the northeast-southwest direction at first. The 630-nm emission poleward of this east-west arc is nearly the background, suggesting that this arc demarcates the polar cap boundary (i.e., the open/closed boundary). Following *Blanchard et al.* [1997], we use the background boundary of 630-nm emission (i.e., the portion where the relative intensity falls to the background level in the polar cap) as a proxy of the polar cap boundary. The white curves in Plates 2i–2q are the polar cap boundaries thus determined. The polar cap boundary associated with the east-west arc is bent at the middle of the field of view, extending northward and westward from there. In addition to this polar cap boundary in the middle, another polar cap boundary is seen in the west of the field of view extending in the north-south direction, as marked in Plates 2i–2q. We see a dark region in the western edge of the field of view. This is also the polar cap. (Note that the dark region on the northwest rim is a shadow of mountains.) Thus the polar cap boundary is not oval-aligned but displaced poleward. As the time sequence shows, there is a vanishing Sun-aligned arc in the region just equatorward of the poleward displaced polar cap boundary. As will be seen in section 5, the decaying Sun-aligned arc is a remnant of the theta aurora that persisted previously in the polar cap. Namely, the poleward expanded portion of the plasma sheet corresponds to the juncture between the transpolar arc and the nightside auroral oval.

The green curves in Plates 1d–1l correspond to the polar cap boundaries determined in Plates 2i–2q, respectively. Here we have assumed an emission altitude of 250 km in the coordinate transformation. From Plates 1d–1l we notice that the sunward flow burst occurred in the region just equatorward of where the polar cap boundary is displaced poleward. Thus we conclude that the flow burst was excited in the outer boundary of the plasma sheet.

A sunward flow burst was also observed in the Southern Hemisphere. Plate 3 shows a time sequence of Doppler velocities obtained by the Halley radar for 0130:12–0149:56 UT, in the same format as that for Plate 1 (east is to the right). The Halley radar was a single-station radar at that time, so here we also discuss exclusively the line-of-sight component. In passing, as in the Goose Bay data, the line-of-sight velocities at lower latitudes (<68°) are largely toward in the eastern part and away in the western part of the field of view, indicating that Halley is also in the eveningside convection cell. At ~0135 UT (Plate 3d) a region of sunward flows appears as indicated by the yellow arrow. We cannot identify the sunward flow region before 0135 UT (Plates 3a–3c), showing that the sunward flow started at ~0135 UT. It grows with time both in its area and in its strength up to ~0144 UT (Plate 3i); then it decays and disappears by ~0148 UT (Plate 3l). Thus the sunward flow burst in the Southern Hemisphere lasted 13 min (0135–0148 UT), which is the same duration as that in the Northern Hemisphere. Note, however, that the start time of the sunward flow in the Southern Hemisphere is delayed by ~7 min compared with that in the Northern Hemisphere.

During the flow burst period in the Southern Hemisphere, DMSP F11 flew over the field of view of the Halley radar from dawnside to duskside and touched the equatorward edge of the sunward flow region at ~0142 UT. The green curve in Plate 3h shows the trajectory of the satellite track. Plate 4 shows energy-versus-time spectrograms of precipitating electrons and ions together with cross-track ion drifts observed by the satellite. The energy-time spectrograms demonstrate that the satellite observed a detached precipitation region in the polar cap (the shaded bar in the top panel of Plate 4). As we see in section 5, a theta aurora was also formed in the southern polar cap in the preceding period, and the detached region in Plate 4 is suggested to be the decaying theta bar observed near the juncture between the theta bar and the nightside auroral oval. The drift meter data show that the theta bar is largely associated with antisunward flows. The satellite transiently crossed a narrow region of sunward flow as marked by the yellow triangle in the top panel of Plate 4. This corresponds to the equatorward edge of the sunward flow (red) region in Plate 3h. Thus the radar and satellite observations are consistent with each other. In order to help the interpretation the satellite orbit and the drift data are also shown in the MLT dial format in Figure 4f, with the shaded region being the theta bar and the solid triangle being the sunward flow region.

We see from Plates 3 and 4 and from Figure 4f that the sunward flow burst in the Southern Hemisphere occurred near the duskward (westward) edge of the theta bar, i.e., in the outer boundary of the plasma sheet as in the Northern Hemisphere. From the same magnetospheric source region and from the same duration time (13 min), we conclude that the sunward flow burst in Plate 3 is the conjugate phenomenon corresponding to that shown in Plate 1. Note that the 7-min time lag is the order of the Alfvén travel time along the magnetic field lines threading the outer boundary of the plasma sheet. This strongly suggests that the location of the flow burst excitation is not in the equator but in the Northern Hemisphere. We should also note that the sunward flow region in the Southern Hemisphere is a very localized structure (~260 km at 400-km altitude) embedded in the large-scale (~1500 km) theta bar associated with antisunward flows, while in the Northern Hemisphere it occupies the entire theta bar with a scale of ~610 km (Plates 1i–1k). This also supports the above idea of the excitation location. From the flow burst timing examined in section 4.3 we will learn that the flow burst was stimulated in or just above the northern ionosphere.

### 4.3. The Timing of the Flow Burst

Now we consider a possible trigger of the sunward flow burst by examining the timing of the flow burst. Figure 3 shows magnetic field perturbations observed on the ground worldwide. The stations are selected to cover the key regions (see Figure 1 and Table 1): the dayside cusp (DRV), the dawnside auroral zone (DIX), and polar cap stations along the theta bar (details in section 5) toward the nightside (ERK, SVS, IGL, and PAN for north; SUD, VOS, and AP3 for south). In terms of the basic two-cell convection, negative excursions in $+D$ at ERK, SVS, IGL, and PAN, in $+Y$ at DRV (after ~0000 UT), and in $-D$ at SUD, VOS, and AP3 all represent enhancements of the antisunward convection in the polar cap. At the same time, negative excursions in $+H$ at DIX and in $-H$ at AP3 represent enhancements of the sunward return flow of the morning and evening cells, respectively. The Geotail observations of MMF B_Z are reproduced at the top but with the
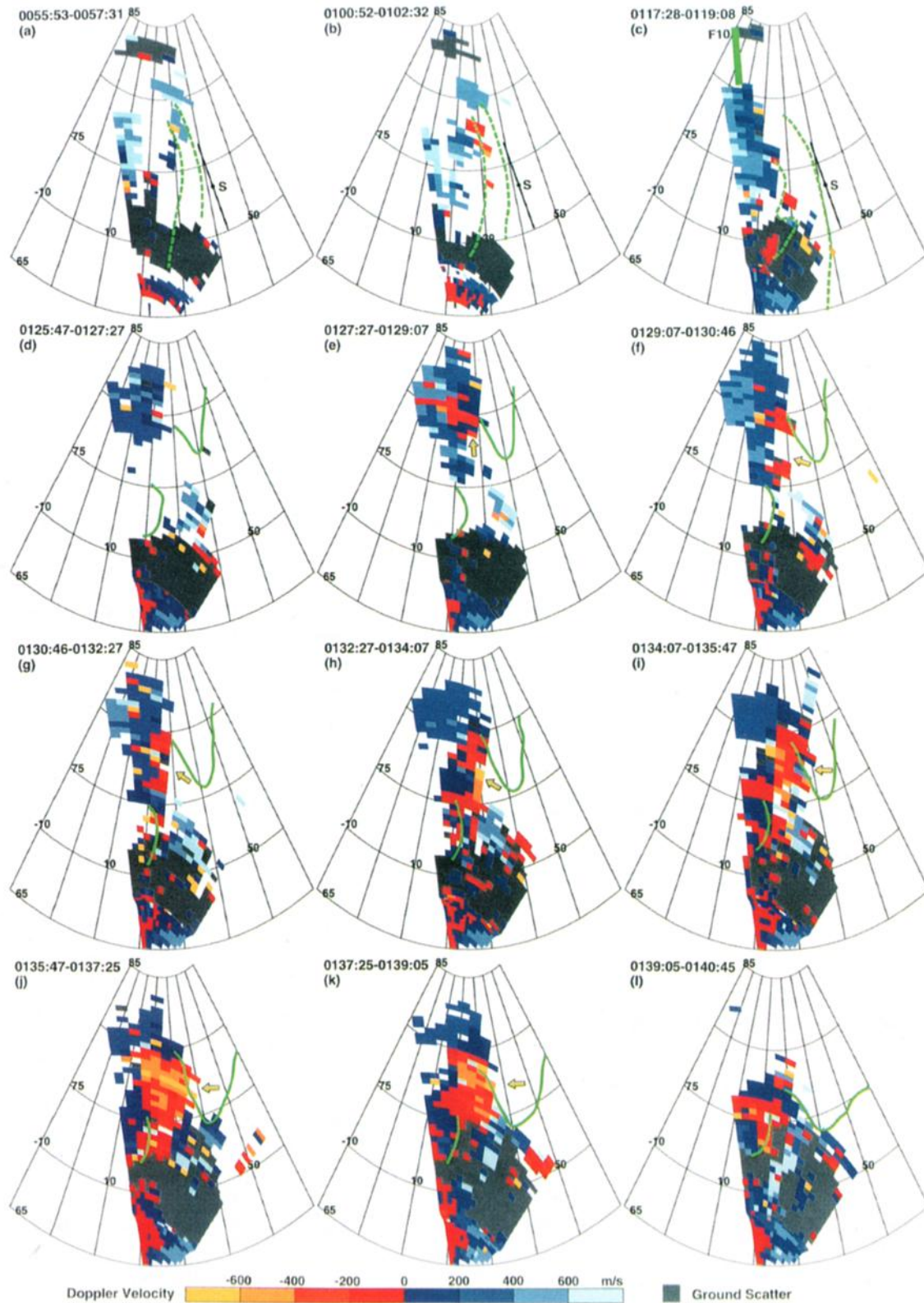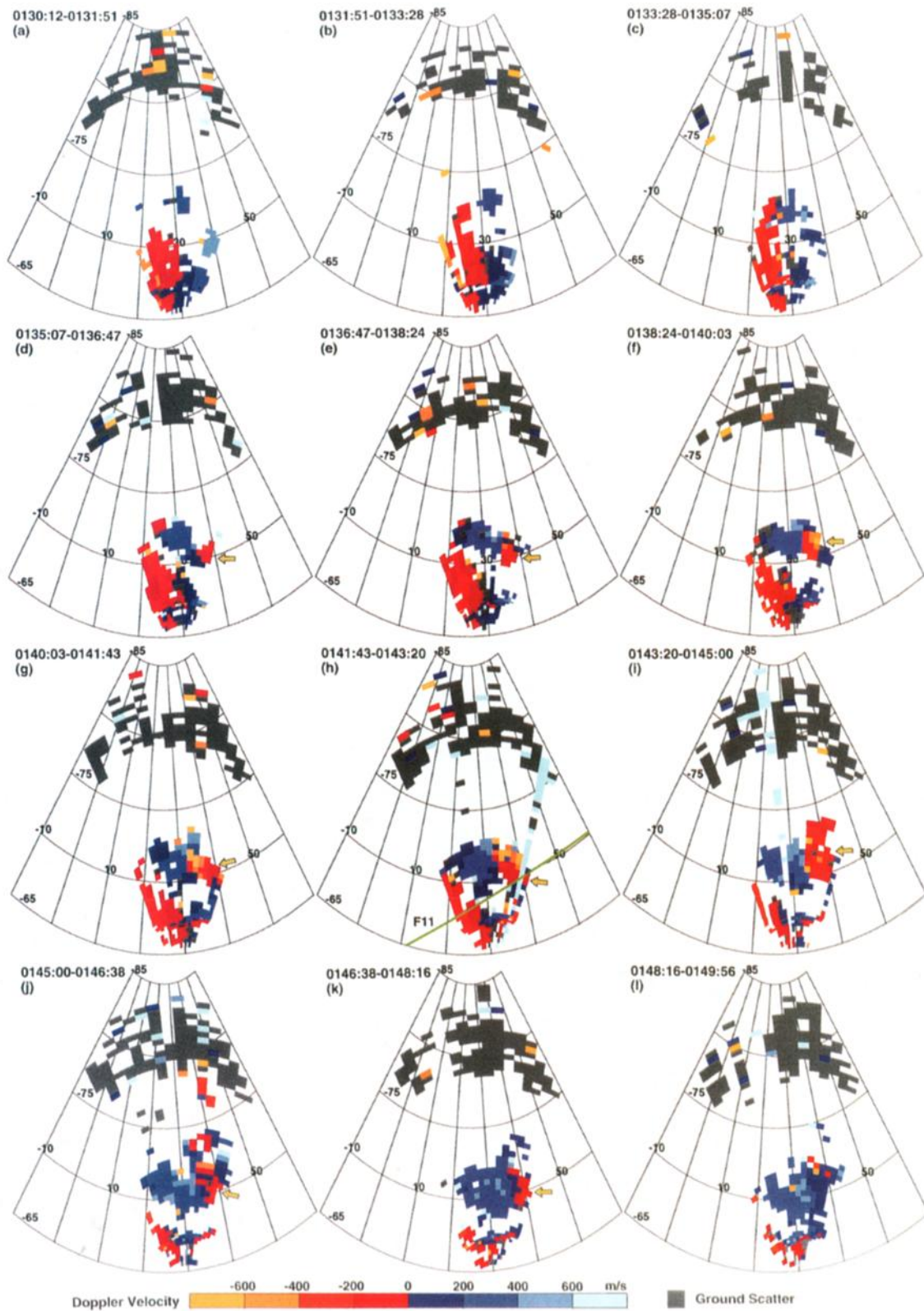
Plate 1. Doppler velocity maps observed by the Goose Bay radar on February 2, 1995: (a–c) selected maps and (d–l) a sequence. Blue represents velocities toward the radar (equatorward), whereas red represents velocities away from the radar (poleward). The green curves in Plates 1d–1l indicate the polar cap boundaries determined from the 630-nm emission in Plates 2i–2q, respectively. The dashed curves in Plates 1a–1c are the easternmost and westernmost edges of the Sun-aligned arc. The green rectangle in Plate 1c is the DMSP F10 observation of the weak flow region (see Figure 4d). The point S in Plates 1a–1c is the location of Søndre Strømfjord with the black line showing the scanning direction of the Sondrestrom IS radar (see Figure 5).
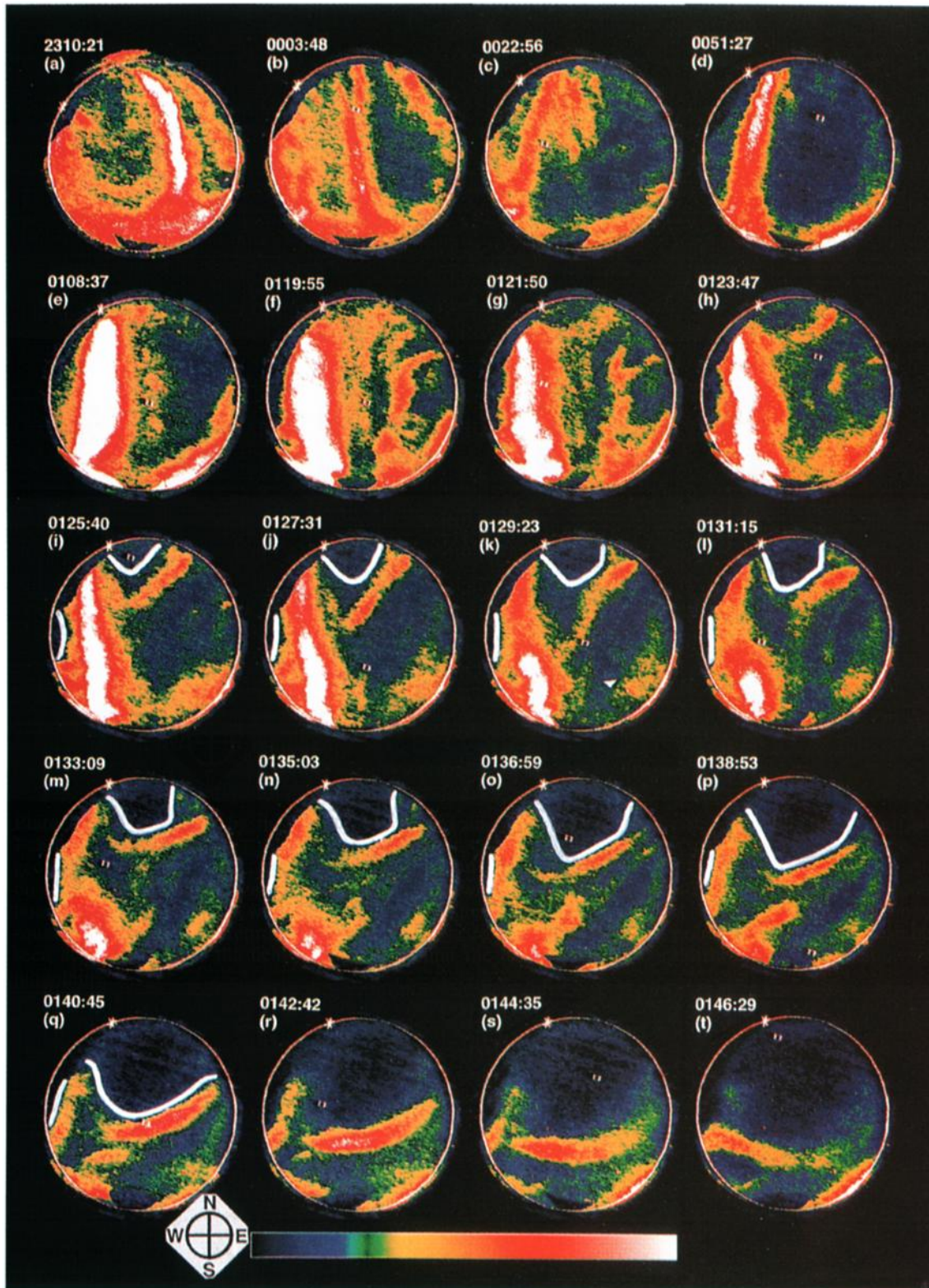
Plate 2. Images taken by the Søndre Strømfjord all-sky camera using the red line filter (630 nm) for February 1–2, 1995: (a–e) selected images and (f–t) a sequence. The top and right of each image is geomagnetic north and east, respectively. The circle on the image represents an 80° zenith angle. The asterisk on the circle shows the azimuth of the Sun. The white curves in Plates 2i–2q indicate the background boundaries of the emission, which correspond to the green curves in Plates 1d–1l, respectively. The small open square in the image field represents the direction toward which the IS radar is pointed. The radar dish can be seen at the bottom of the field of view. Note that the dark region on the northwest rim is a shadow of mountains.

Plate 3. (a–l) A time sequence of Doppler velocity maps observed by the Halley radar on February 2, 1995, in the same format as that for Plate 1 (east is to the right). The green curve in Plate 3h is the track of DMSP F11 (see Figure 4f and Plate 4).
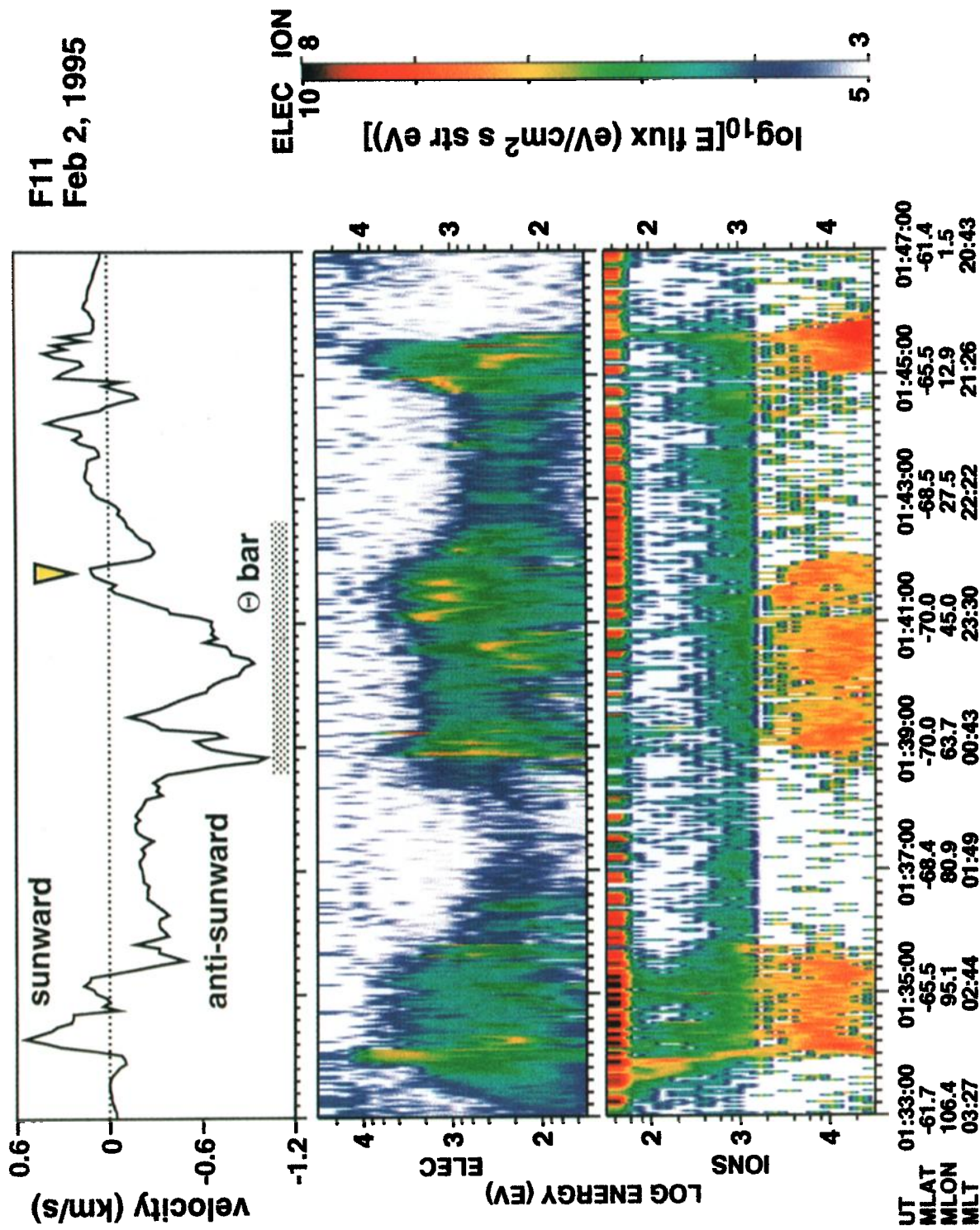
Plate 4. Observations by DMSP F11 during the flight over the field of view of the Halley radar (see Plate 3h):(top) the cross-track component of horizontal ion drift velocities and (middle and bottom) energy-versus-time spectrograms of precipitating electrons (middle, energy increasing upward) and ions (bottom, energy increasing downward). The shaded bar in the top panel shows the period of the "theta bar" observation.
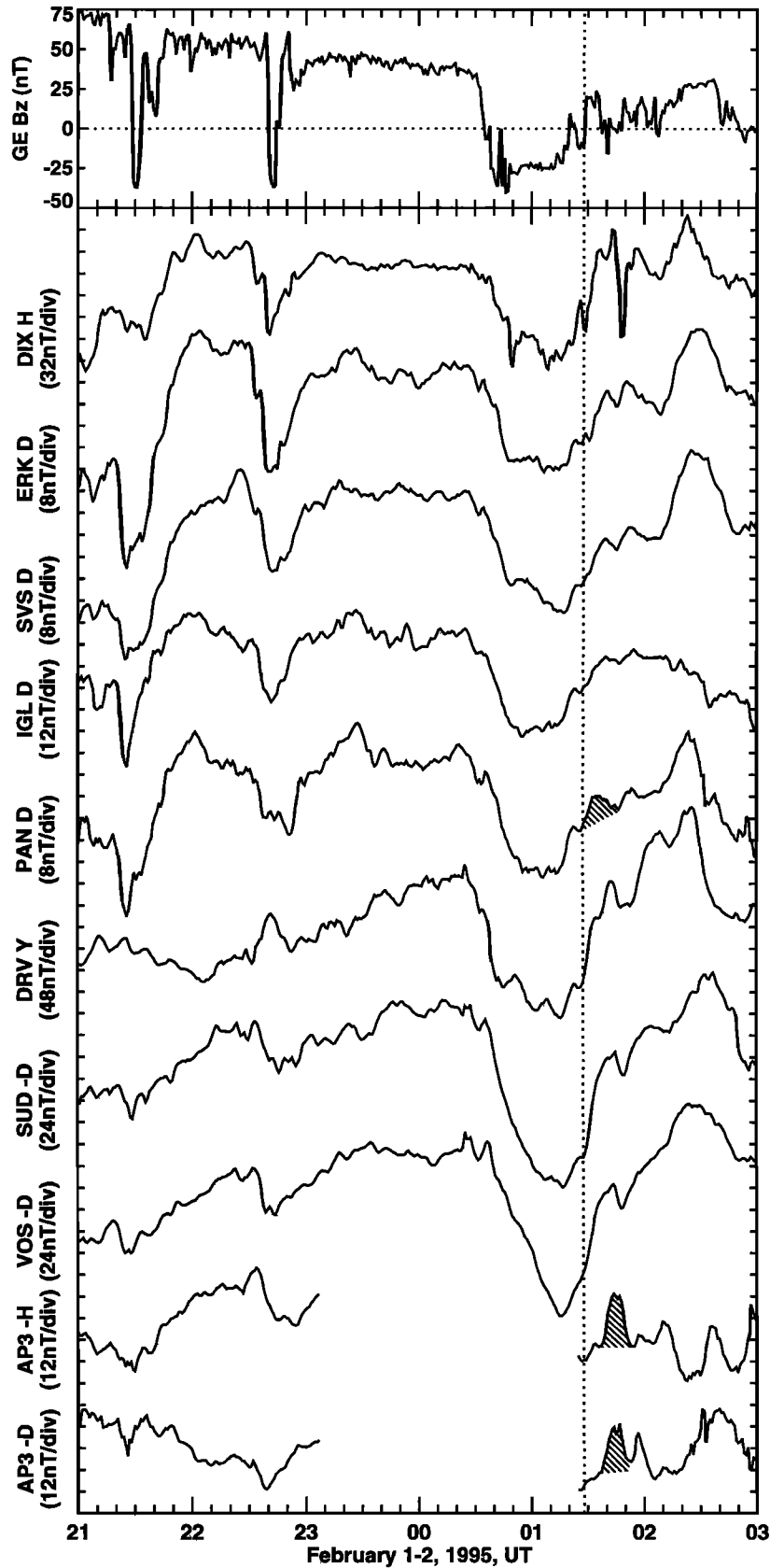
Figure 3. Magnetic field perturbations on the ground, together with (top) Geotail observations of MMF B_Z with the time axis shifted forward by 8 min. DIX, Dixon; ERK, Eureka; SVS, Savissivik; IGL, Igloolik; PAN, Pangnirtung; DRV, Dumont d'Urville; SUD, Sude; VOS, Vostok; AP3, Automatic Geophysical Observatory (AGO) P3. Note that $-D$ or $-H$ is plotted for Sude, Vostok, and AGO P3. AGO P3 data have a gap for 2307–0125 UT.

abscissa shifted forward by 8 min in order to demonstrate the similarities between the interplanetary and ground observations. Note that the time shift in the Geotail data was determined by doing a cross correlation on the data from Geotail against the DIX H and ERK D data during the 2200–0200 UT period, resulting in time lags of 8 and 9 min, respectively. Examination of Figure 3 reveals that the variations on the ground are well synchronized with Geotail B_Z. Such worldwide geomagnetic fluctuations well correlated with IMF B_Z are known to be DP 2 fluctuations [*Nishida*, 1968].

Pangnirtung (PAN) and AGO P3 (AP3) were the nearest stations in the Northern and Southern Hemispheres, respectively, to the sunward flow bursts. In the Northern Hemisphere the sunward flow burst occurred at 0128–0141 UT. At the peak of the flow enhancement observed by the Goose Bay radar, PAN was located at the southwestern edge of the sunward flow region (Plates 1j and 1k). During the flow burst period the D disturbance at PAN shows a positive excursion consistent with the sunward flow (the hatched portion in Figure 3). However, this positive excursion is weak against the large positive trend of the variation, so we cannot conclude that it really detected the sunward flow burst. It may be that PAN was not directly under the sunward flow region. In contrast, in the Southern Hemisphere we can clearly identify the bursty feature of the sunward flow for 0135–0148 UT. AP3 was situated just beneath the sunward flow region observed by the Halley radar (Plates 3d–3k). The $-H$ and $-D$ disturbances at AP3 clearly show positive excursions during the sunward flow interval (the hatched portions in Figure 3), indicating that the flow is sunward and eastward.

The vertical dotted line in Figure 3 shows the start time of the sunward flow in the Northern Hemisphere (0128 UT). The sunward flow continued 13 min from this time. We notice that the sunward flow onset in the Northern Hemisphere is well synchronized with the positive B_Z excursion, which actually passed Geotail in the magnetosheath at 0121 UT (the dashed line in Figure 2i). This strongly suggests that the flow burst was triggered by the positive B_Z transition. In addition, the ground magnetic signature that corresponds to the positive B_Z excursion is observed worldwide almost simultaneously (within 1 min) at 0128 UT. For example, we cannot discern a significant difference in the response time between the dayside cusp region (DRV) and the nightside flow burst region (PAN). Since magnetometers measure integrated effect of any currents, it might be that they detected currents far away from the observatories. However, we checked that this is not the case by comparing the magnetometer disturbances at PAN and the radar line-of-sight velocities in a region to the west of the northern flow burst; the variations were quite similar to each other, indicating that the magnetometer data in Figure 3 do indeed express the local ionospheric currents above the observatories. Therefore we conclude that the signal of the positive B_Z transition pervaded the entire polar cap instantaneously, triggering the sunward flow burst in the Northern Hemisphere.

We now estimate the arrival time of the B_Z transition signal at the dayside magnetopause using a magnetosheath flow model, with a simple assumption that the magnetic field perturbations are convected through the magnetosheath at the local plasma velocity. The upstream sonic Mach number (MA) in this event ranged from 8 to 10 and did not show drastic changes (see Wind observations in Figures 2a–2c). We compared upstream Wind and downstream Geotail observations and found that the axisymmetric gas dynamic model for MA =

8 calculated by *Spreiter and Stahara* [1980] predicted the downstream magnetosheath plasma flow to a remarkable degree. Therefore we adopted Spreiter and Stahara's model in the estimation. In the application of their model we have added one improvement. It is known that the gas dynamic model breaks down in the very vicinity of the magnetopause. The gas dynamic model assumes that the magnetopause is a tangential discontinuity and hence that there are no plasma flows crossing the boundary. In reality, however, the normal component of the plasma flow at the subsolar magnetopause is ~20 km/s [*Phan et al.*, 1994]. Therefore, in the estimation we assumed that the flow along the X axis decreased down to not zero but 20 km/s at the magnetopause.

The sharp positive excursion in Geotail B_Z occurred from 0120:05 to 0120:35 UT (high-resolution data). Assuming the signal front in the upstream to be perpendicular to the X axis, we calculate the time lag between the B_Z signal being detected at Geotail and its arrival at the subsolar magnetopause to be 275 ± 5 s (errors are those from the digitization and interpolation of the original figures of Spreiter and Stahara [1980]). Namely, the signal arrives at the subsolar magnetopause at 0125:10 UT. The signal front may not be perpendicular to the X axis. The B_Z transition passed Wind at 0102 UT ((X, Y, Z) = (187.0, −49.8, −32.7) R_E) and reached Geotail at 0121 UT ((11.4, 4.0, 2.7) R_E) as marked by dashed lines in Figures 2f and 2i. The 19-min time lag is much shorter than that expected from the X distance between the two satellites and from the observed solar wind speed, but it is explainable if the normal direction of the signal front is 54° off the X axis in the X-Y plane (i.e., Parker spiral approximation). In this case, the time lag between Geotail and the subsolar magnetopause becomes 321 ± 5 s. That is, the estimated arrival time is 0125:56 UT. Accordingly, considering some ambiguity, we conclude that the IMF B_Z signal reached the subsolar magnetopause at 0125–0126 UT.

Thus the estimated arrival time of the B_Z signal is 0125–0126 UT, while on the ground the signature of the ionospheric response starts at 0127–0128 UT in the entire polar cap as marked by the dotted line in Figure 3. This 2–3 min time lag compares with the Alfvén travel time from the dayside magnetopause to the ionospheric cusp. This suggests that on arriving at the dayside cusp ionosphere the B_Z signal is transmitted to the nightside ionosphere instantaneously. Note also that 2–3 min is not enough for the fast mode wave in the magnetosphere to propagate to the nightside plasma sheet and then for the Alfvén wave to travel down into the nightside ionosphere. Therefore the simultaneous onsets of the ionospheric response and the flow burst in the Northern Hemisphere indicate that the excitation of the flow burst occurred in or just above the northern ionosphere.

5. Evolution of the Polar Cap Prior to the Flow Bursts: Preconditioning of the Magnetosphere

We have examined the sunward flow bursts and their possible cause. The IMF B_Z transition is suggested to have triggered the sunward flow in the Northern Hemisphere. However, the excitation of the flow burst was brought about not only by the external source but also by the internal condition that made the magnetosphere susceptible to the external jolt. Namely, the magnetosphere retained the "memory" of the preceding IMF B_Z northward condition. In sections 5.1–5.4 we

examine the magnetosphere-ionosphere system prior to the sunward flow bursts by visualizing the evolution of the polar cap.

5.1. The Stable and Northward MMF Period (2300–0025 UT in the Ionosphere)

Up until 0022 UT, MMF B_Z was stable and northward (Figure 2i). The subsequent southward excursion of B_Z did not appear in ground magnetometer signatures until at least 0025 UT (Figure 3). Figure 4a shows combined observations over the northern dayside ionosphere from F11 and F12 and over the southern nightside ionosphere from F11 and NOAA 12 during the time interval from ~2300 to 0000 UT. During the stable and northward MMF period, theta auroras (transpolar arcs) were found in both northern and southern polar caps. At ~2328 UT, NOAA 12 crossed a region of precipitating electrons and ions forming the part of the theta bar in the Southern Hemisphere, as shown shaded at premidnight. Similarly, F11 and F12 observed the theta bar in the Northern Hemisphere at ~2307 and ~2336 UT, respectively, as shaded at dayside high latitudes.

The presence of the theta aurora was also observed on the ground in the northern polar cap. Plates 5a–5c are all-sky images during the stable and northward B_Z period obtained at Eureka using a 558-nm filter. Plate 5c is an observation just before the effects of the southward excursion of B_Z started on the ground. A transpolar arc came into the field of view of the camera from the duskside rim at ~2310 UT, February 1, 1995, and migrated toward the center of the image gradually. For 2330–2340 UT the arc was still located duskward of Eureka (Plate 5a), which is consistent with the DMSP F12 observation at ~2336 UT in Figure 4a. The MMF obtained by Geotail (Figures 2g–2i) shows that there was a negative B_Z spike at ~2234 UT associated with a negative B_Y excursion, following a long (>1 hour) period of stable northward B_Z. We infer that this B_Z spike triggered the formation of the transpolar arc on the duskside, as discussed in section 6.2. Then at ~2348 UT another arc starts to extend from the dayside on the dawnside of the preexisting arc, and the theta bar forms a well-defined double arc (Plate 5b). The double arc, varying in luminosity, develops over Eureka (Plate 5c).

Figure 4a also displays cross-track ion drift data obtained by F11 in the dayside (Northern Hemisphere) and nightside (Southern Hemisphere) flights. On the dayside the plasma convection is a four-cell pattern with sunward flows at magnetic latitudes >80° [e.g., *Heppner and Maynard*, 1987]. In contrast, on the nightside the flow direction changes randomly at magnetic latitudes >70° and does not display a well-defined flow pattern. These features are a typical convection pattern for northward IMF B_Z [e.g., *Bythrow et al.*, 1985]. It would be useful to note here that the transpolar arc (or theta bar) is collocated with a region of velocity shear for both hemispheres (for the Southern Hemisphere we combine the NOAA 12 particle and F11 drift data assuming the arc is Sun-aligned). That is, the arc appears at the region of electric field convergence [e.g., *Carlson et al.*, 1988].

Plates 2a–2c are examples of all-sky images in the red line (630 nm) obtained at Søndre Strømfjord during the stable northward B_Z period; Plate 2c is the image just before the effects of the southward excursion of MMF B_Z started on the ground. In the premidnight region, multiple Sun-aligned arcs are observed as Plates 2a–2c, with the nightside edge of the major arc connected with the auroral oval. By transforming the images of Plates 2 and 5 into a common coordinate system, and

by considering the time sequence of the auroral motion, we confirmed that the major Sun-aligned arc in the middle field of view in Plate 2 is the extension of the duskside component of the double transpolar arc in Plate 5. The emission on both sides of the major Sun-aligned arc is usually above the background level, so we infer that the field of view of the all-sky camera was entirely in the closed magnetic field region. Poleward moving auroral structures were often found, which is consistent with the IS radar observation in Figure 5. Figure 5 shows ion drift velocities in the STF geomagnetic meridian (see Figure 1a). The velocities at magnetic latitudes >75° are preferably poleward after ~2220 UT.

5.2. The Southward Excursion of the MMF and the First Half of the Southward MMF Period (0025–0055 UT in the Ionosphere)

From 0022 to 0033 UT, MMF B_Z exhibited a southward excursion and changed its sign from +33 nT to −37 nT, and after that, a southward B_Z period continued up until 0112 UT (0120 UT in the ionosphere; see Figures 2i and 3). The plasma flow at dayside high latitudes becomes antisunward as shown in Figure 4c (northern F11 overflight for 0040–0100 UT), which contrasts with the four-cell convection pattern for the stable and northward B_Z period (Figure 4a). We divide this southward B_Z period into two, because the auroral behavior on the nightside is different. In this section we treat the first half, i.e., the period until ~0055 UT.

The transpolar arcs in the polar cap do not decay immediately in response to the southward turning of the MMF. Figure 4b shows nearly simultaneous observations of the southern polar cap by F10 and F12 during the southward B_Z transition. Both satellites crossed a region of precipitating electrons forming the part of the theta bar at high latitudes (>80° MLAT) on the midnight meridian (the shaded region in Figure 4b). Drift meter data from F12 show weak but appreciable sunward flows throughout most of the nightside pass. (No drift meter data were available from F10 for this polar pass.) As for the large-scale features on the nightside, those for the northward B_Z period are still persisting at this stage.

Plates 5d–5f demonstrate the decaying process of the northern transpolar arcs observed at Eureka. Plate 5d is an image during the southward B_Z transition. The dawnside component of the previously developed double arc starts to disappear, although it is not clear that this is because of the MMF southward turning. The disappearance occurs first overhead and then on the nightside. The dayside part of the arc persists a little longer, but it finally fades out by ~0040 UT. In contrast, the duskside component of the double arc survives a while, drifting dawnward and tilting in the dawn-dusk direction (Plate 5e). Thereafter the arc retreats antisunward (Plate 5f) and leaves the field of view of the camera around 0105 UT. Thus the antisunward decay of the major transpolar arc does not start until 30–40 min after the southward turning of the MMF.

Plate 2d shows how the Sun-aligned arcs in the premidnight sector evolved after the southward turning of the MMF. A salient feature when compared to Plate 2c is that the auroral structures attached to the major Sun-aligned arc have disappeared, and the emissions on both sides of the major arc have fallen to nearly the background. Since the 630-nm emission is sensitive to weak electron precipitation and is often used as a diagnosis tool of the polar cap boundary [*Blanchard et al.*, 1997], these observations suggest that both sides of the major Sun-aligned arc are likely to be on open magnetic field lines.
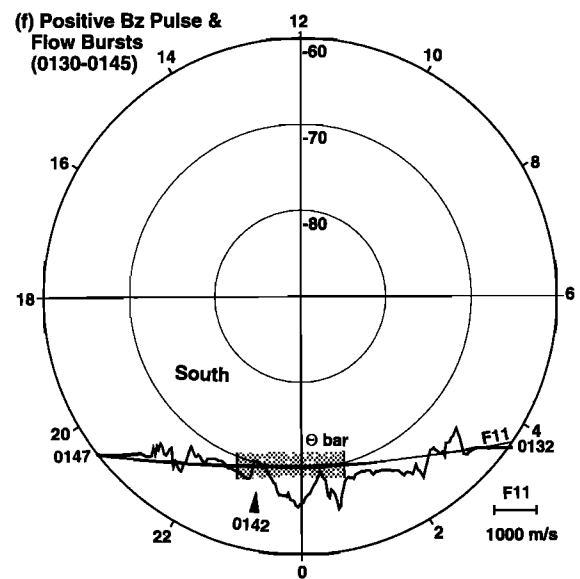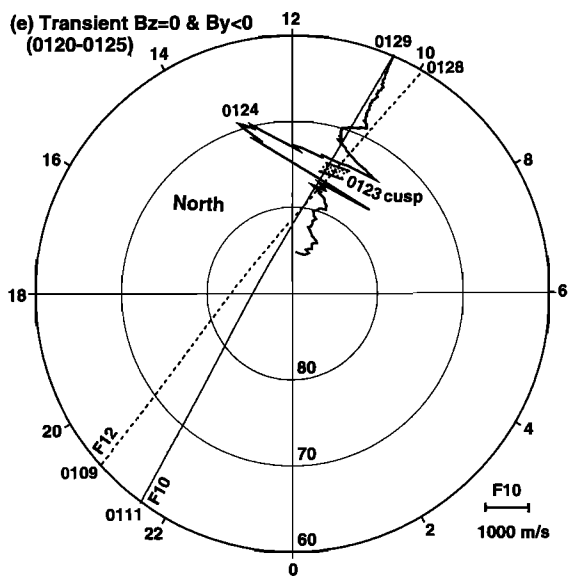
(a) Stable & Northward Bz (2300-0000)

(b) Start of Bz Negative Excursion (0025-0035)

(c) Southward Bz (0040–0100)

(d) Southward Bz (0110-0120)

(e) Transient Bz=0 & By<0 (0120-0125)

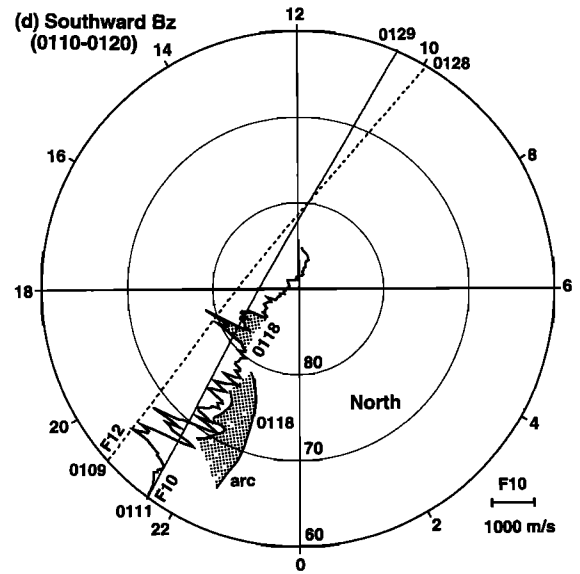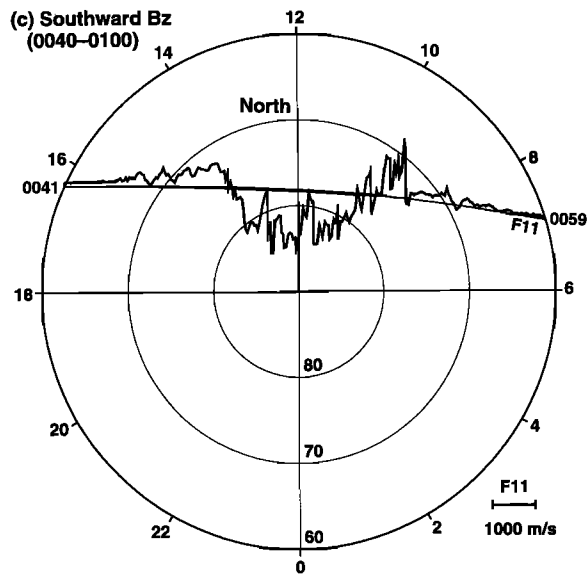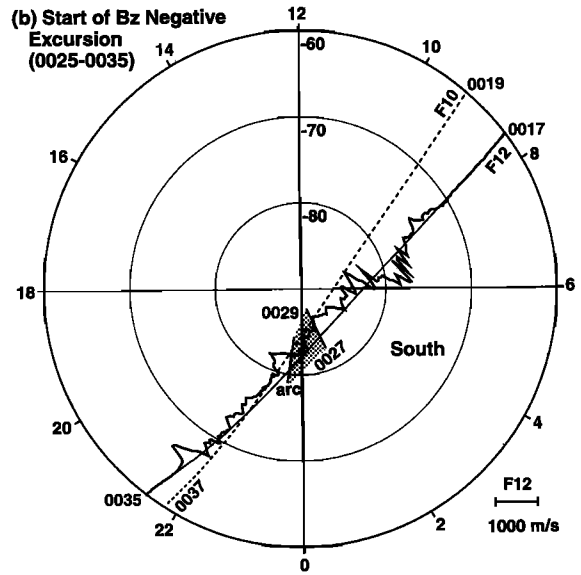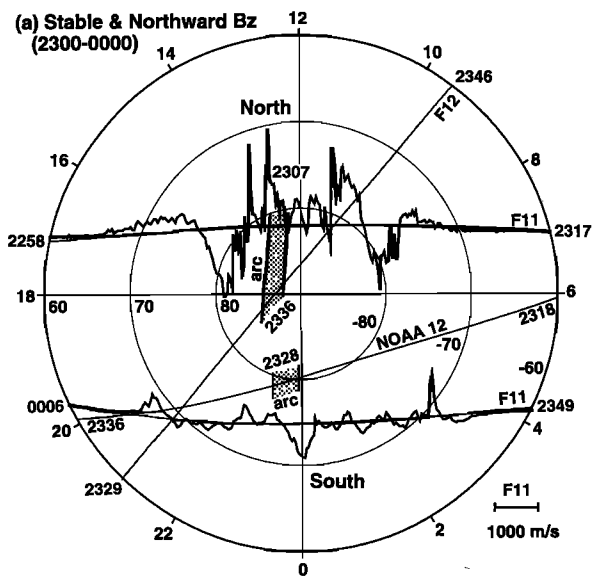(f) Positive Bz Pulse & Flow Bursts (0130-0145)

Figure 5 indicates that the plasma convection to the east of the Sun-aligned arc turned equatorward (i.e., antisunward) by ~0040 UT. The filling up of either side of the arc with open magnetic flux would be related to this convection change.

5.3. The Second Half of the Southward MMF Period (0055–0120 UT in the Ionosphere)

As described in section 5.2, the Sun-aligned arc on the night-side becomes very thin and well defined by 0050 UT (Plate 2d). However, from ~0055 UT the Sun-aligned arc starts to lose its shape. Plates 2e and 2f are two examples that show the changes. The Sun-aligned arc broadens longitudinally compared to Plate 2d, and once again both sides of the arc are filled with emissions by 0115 UT. At the same time the arc rotates counterclockwise. The reappeared emission on both sides of the arc implies that regions of closed magnetic field lines expanded to the east and west of the arc.

From ~0050 UT the Goose Bay radar started to receive good ionospheric echoes (prior to that, no good echoes returned). Plates 1a–1c are selected examples. The dashed green curves show the eastern and western edges of the Sun-aligned arc observed by the all-sky camera at Søndre Strømfjord (the corresponding images are not shown in Plate 2). Unfortunately, echoes returned exclusively from the western side of the arc, except for a few examples. On the western side of the arc the plasma flow is toward the radar (or equatorward) throughout as shown in Plates 1a–1c. On the eastern side of the arc the Sondrestrom IS radar was operating; the point S in Plates 1a–1c is the location of Søndre Strømfjord. Figure 5 reveals that the flow direction changed from poleward to equatorward at ~0030 UT, and after that, the plasma flow is persistently equatorward at all latitudes. The black line passing through the point S in Plates 1a–1c shows the plane of IS radar observations in Figure 5. The Goose Bay and Sondrestrom radars thus show that the flow is equatorward on either side of the Sun-aligned arc.

For ~0100–0105 UT the Goose Bay radar fortuitously detected a few echoes over the Sun-aligned arc as shown in Plate 1b. We see patchy echoes of a sunward flow region (red) along the western border of the Sun-aligned arc. In contrast to antisunward flows on both sides of the arc, sunward flows are not entirely extinct over the arc even 40 min after the southward turning of the MMF. This would be the origin of the subsequent bursty enhancement of sunward flows.

Figure 4d shows DMSP observations in the premidnight sector for 0110–0120 UT. F10 and F12 traversed nearly synchronously (2 min apart) in the 2000–2200 MLT sector (the F12 orbit is shown dashed). (The drift meter data after 0121:14 UT are shown in Figure 4e separately.) Unfortunately, only the drift meter data from F10 and the particle data from F12 were available during this pass. However, this was enough data to provide useful information for our interpretation. At ~0118 UT the F10 satellite observed an isolated region of weak flows in the polar cap (>80° MLAT, the shaded region of the F10 drift meter data in Figure 4d) bounded by antisunward flow

regions. The orbital segment of this region is superimposed on the simultaneous radar observations in Plate 1c (the green rectangle at the top). In Figure 4d the aurora arc observed on the ground at ~0118 UT (the same as in Plate 1c) is shown for reference. Although no F10 particle data were available, the isolated weak flow region in Figure 4d and Plate 1c is thought to be the continuation of the nightside Sun-aligned arc observed on the ground. It is worth noting here that along the F12 orbit in earlier MLTs (the dashed line in Figure 4d) no signature of Sun-aligned arc precipitation was found. This means that the Sun-aligned arc is absent or bent dawnward at antisunward of the dawn-dusk meridian. This is consistent with the Eureka all-sky observation: The transpolar arc decayed antisunward and became indiscernible in the field of view of the camera around 0105 UT.

5.4. Just Before and During the Positive B_Z Pulse (0120 UT Onward)

Just before the MMF B_Z pulse, there was a period of weak B_Z. Figure 4e is the continuation of Figure 4d (0121:14 UT onward) and corresponds to the observations during this weak B_Z period. Although, as noted in section 5.3, only the drift meter data from F10 and the particle data from F12 were available, the close approach of the two satellites, both in space and time, enables us to combine the two data sets. We see a strong duskward flow (the F10 observation at 0124 UT) associated with the prenoon cusp (the F12 observation at 0123 UT). The MMF B_Y was negative during this period, so we infer that this duskward flow is a consequence of IMF B_Y effects reported by many authors [e.g., Heppner and Maynard, 1987]. Thus, on the dayside, effects of the real-time IMF change are discernible. On the nightside, however, a full-scale effect of the preceding southward B_Z period has started.

We now reexamine Plates 2f–2t, i.e., a time sequence of Søndre Strømfjord all-sky images before and during the sunward flow burst observed by the Goose Bay radar. As noted in section 5.3, emissions have reappeared on both sides of the Sun-aligned arc and have filled the entire field of view of the camera by 0115 UT. After ~0118 UT the emissions to the west of the arc fade to near the background as seen in Plate 2f, indicating that the region to the west of the arc has been occupied by open magnetic flux once again. (Note that a shadow of mountains appears on the northwest rim of the images in Plate 2.) At this stage the region to the east of the arc is still filled with emissions. Around 0122 UT (Plate 2g) an arc perpendicular to the Sun-aligned arc enters the field of view in the north and migrates equatorward with time to the east of the Sun-aligned arc (Plates 2h–2t). This arc demarcates the polar cap boundary as shown by white lines in Plates 2i–2q. The equatorward motion of the east-west arc is consistent with the Sondrestrom IS radar observations in Figure 5. The ion drift in the geomagnetic meridian is persistently equatorward even after the arrival of the positive B_Z pulse (0127 UT), although some indication of weakening is seen around 0125 UT. Equatorward motion of the polar cap boundary is a signature of the substorm growth phase. It is suggested that although B_Z already turned northward, effects of southward B_Z are still dominant on the nightside.

During the equatorward migration of the polar cap boundary, the Sun-aligned arc fades away gradually and finally disappears at ~0148 UT. However, when the B_Z pulse reaches the ionosphere (0127–0128 UT), the Sun-aligned arc is still active (Plate 2j), and as discussed in section 4.2, the sunward

Figure 4. (opposite) (a–f) Evolution of the polar cap inferred from precipitating particles or cross-track ion drift obtained by four polar-orbiting satellites. The ion drift is shown along the spacecraft orbit (the reference is the satellite track). The four-digit numerals indicate approximate UTs. Key regions such as Sun-aligned arcs and the cusp are shown shaded.
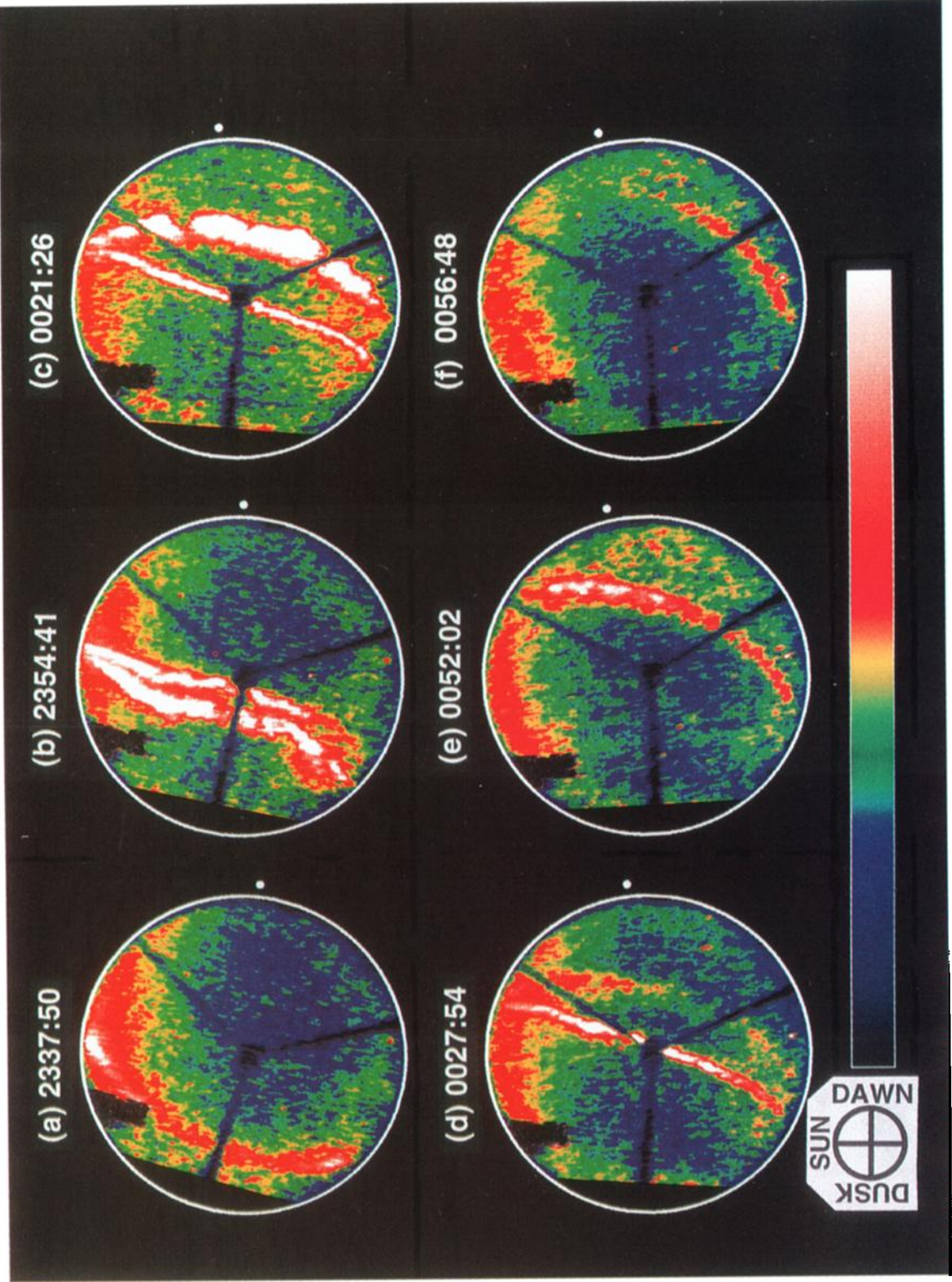
Plate 5. (a–f) Selected images taken by the Eureka all-sky camera using the green line filter (558 nm) for February 1–2, 1995. The top and right of each image correspond to sunward and dawnward, respectively. The white circle on the image represents an ~90° zenith angle. The white dot outside the circle shows the magnetometer +D direction (see Figure 3). Note that the shadow of the three-pronged camera leg is seen in the image field. The dark regions at the left and at the upper left of the field of view are artificial shadows caused during the videotape recording.
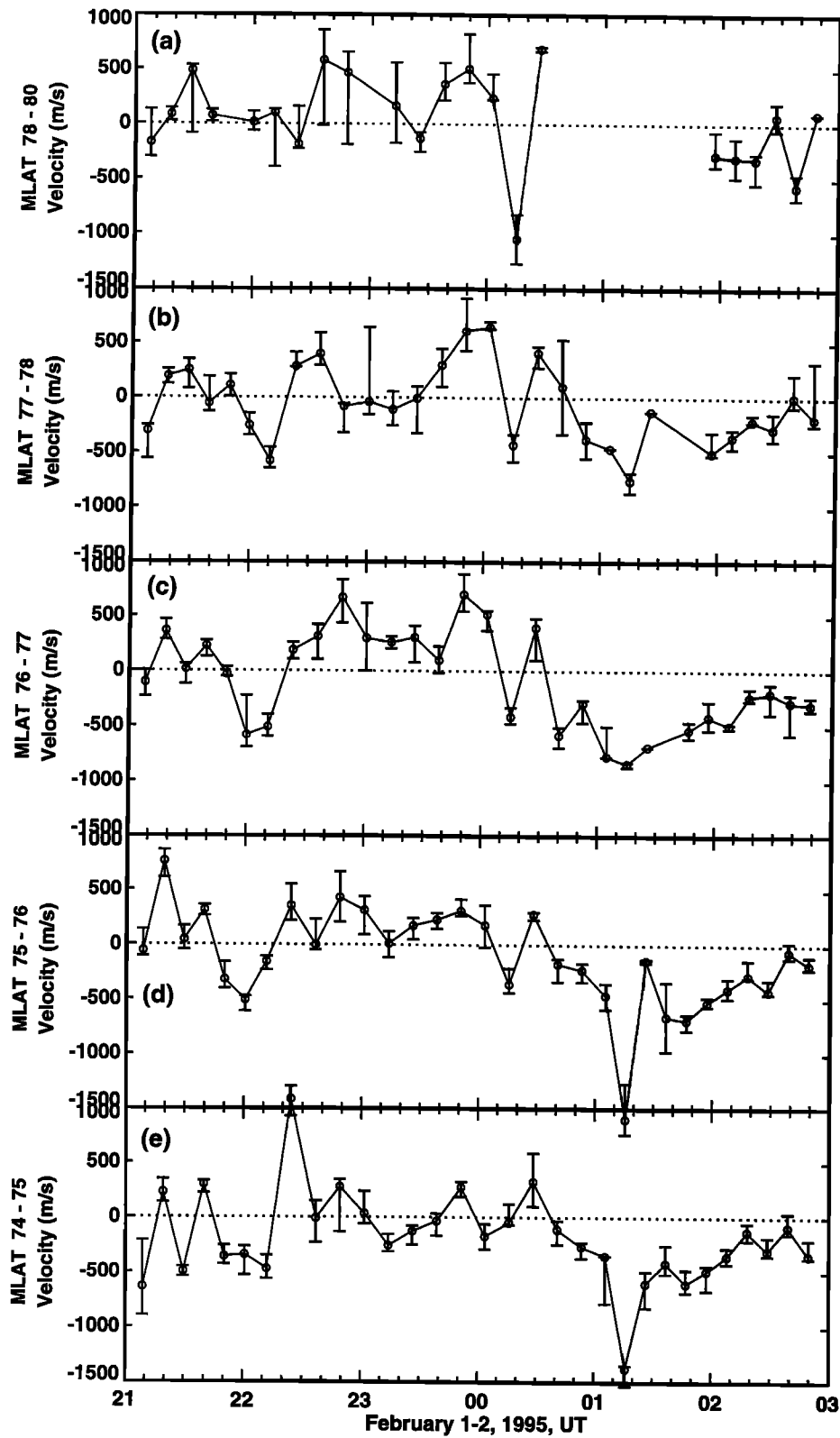
Figure 5. (a–e) Ion drift velocities at 300-km altitude in the Søndre Strømfjord geomagnetic meridian (positive northward; see Figure 1a and Plates 1a–1c) determined from the Sondrestrom IS radar. The three quartiles (the median and the upper and lower quartiles) in each MLAT bin are shown.

flow burst occurred in the region just equatorward of where the remnant of the theta aurora causes the polar cap boundary to be displaced poleward. It is suggested that the sunward flow channel is still active at this time (section 5.3). Thus we conclude that the remnant of the sunward flow channel in the northern ionosphere is the origin of the sunward flow burst. As we saw in section 4.2, this sunward flow burst was also observed in the Southern Hemisphere at the duskside edge of the decaying theta aurora (Figure 4f) but with a 7-min delay from the Northern Hemisphere.

6. Discussion

6.1. Ionospheric Source?

Let us consider here the possibility of the sunward flow bursts being produced not by reconnection processes in the magnetosphere but by collision-dominated processes in the ionosphere. We examine two possibilities: (1) effects of ionospheric conductivities and (2) the drag of the neutral wind.

Strong electron precipitation, such as that associated with the onset of the substorm expansion phase, ionizes the E region and enhances the ionospheric conductivity. There are several reports in the literature which suggest that the ionospheric conductivity modifies the electric field pattern and produces flow bursts [e.g., Morelli et al., 1995]. A high-conductivity region creates an obstacle which diverts the background flow around it, and the diverted flow is accelerated. This process, however, is unlikely in this case. In the all-sky images at Søndre Strømfjord (Plate 2) we cannot discern any signatures of strong electron precipitation around the sunward flow region. In Plate 4 we see weakly accelerated electrons (peak energy ≈ 1.5 keV, energy flux $\approx 1.6 \times 10^8$ eV cm^{-2} s^{-1} sr^{-1} eV^{-1}) to the east of the sunward flow region in the Southern Hemisphere; however, the energy flux is not sufficient to ionize the E region to enhance the conductivity dramatically [e.g., Banks et al., 1974]. In addition, the 7-min onset time lag between the two hemispheres is too long for the particle fluxes from the same source region in the magnetosphere.

Next we consider the drag of the neutral wind. The sunward flow speed in the Northern Hemisphere exceeds 600 m s^{-1} (Plate 1j). Although the E region neutral wind speed is typically 100 m s^{-1} or less, at F altitudes it could reach such a high speed. We should note, however, that the time constant of the sunward flow ($\sim$6 min, for both growth and decay) is much smaller than that of the neutral wind (typically 1–2 hours); for instance, Thayer et al. [1995] determined the time constant of the neutral wind in the polar cap experimentally for two cases: 117 min for one case and 41 min for the other case. It is, in general, impossible to drive the neutral wind up to 600 m s^{-1} within several minutes whatever the source may be. In addition, the neutral wind in the polar cap is always affected by the antisunward pressure gradient force that compares the collisional force [Thayer et al., 1995]. Therefore the neutral-wind-driven sunward flow is also unlikely.

6.2. A Possible Scenario

Here we propose a possible scenario that explains the formation of the sunward flow bursts; it would also serve as an observational summary. Figure 6 schematically illustrates the polar cap evolution inferred from the coordinated observations. The closed curve shows the polar cap boundary, i.e., the open/closed boundary. The solid arrows represent plasma motion; the shaded regions are auroral arcs.
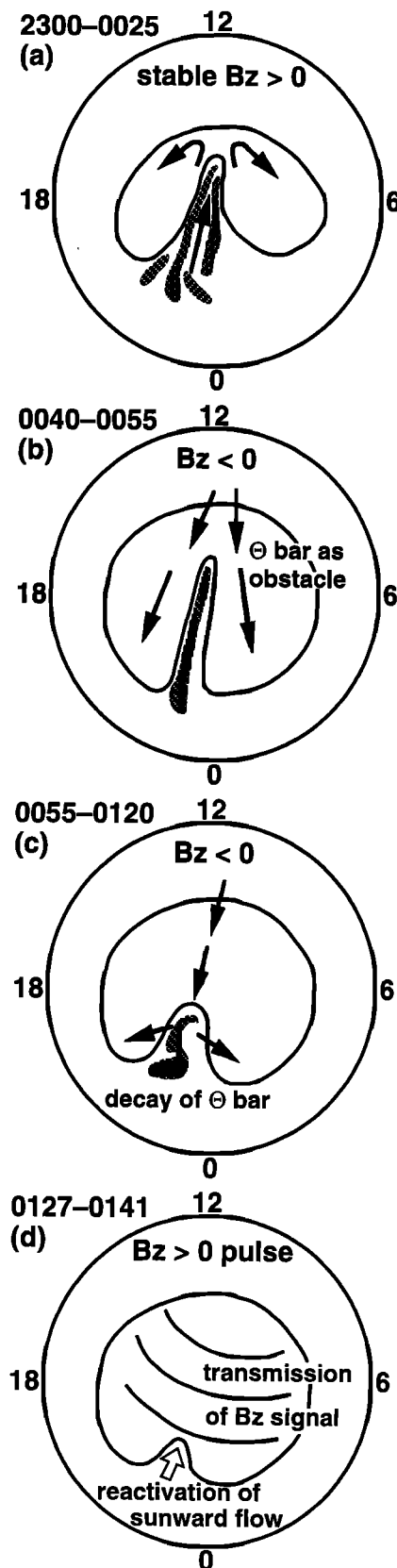
Figure 6. (a–d) A schematic summary of the polar cap evolution prior to the sunward flow bursts.

During the period of stable and northward B_Z prior to 0025 UT, a theta aurora was formed in the northern polar cap (Figure 6a). At first, one transpolar arc emerged on the duskside and drifted dawnward across the polar cap to form the theta bar. It has been suggested that a crucial factor for the theta aurora formation is transient polarity changes in B_Y or B_Z after a long period of northward IMF [Newell and Meng, 1995; Cumnock et al., 1997; Chang et al., 1998]. Geotail observations (Figures 2g–2i) indicate that there was a negative B_Z spike at ~2234 UT associated with a negative B_Y excursion, following a long (>1 hour) period of stable northward B_Z. We suspect that these B_Y and B_Z changes for 2230–2250 UT (Geotail observations) are the trigger of the theta aurora. The above cited previous studies on theta aurora formation indicate that the transpolar arc starts on the duskside (dawnside) auroral oval for negative (positive) B_Y and drifts dawnward (duskward) across the polar cap in the Northern Hemisphere (and conversely in the Southern Hemisphere). The Eureka observations of the dawnward drifting transpolar arc that followed the negative B_Y excursion are consistent with this conjecture. Since the MMF is due northward after the B_Y change, well-defined theta auroras are expected to form in both hemispheres.

Then the theta bar became a double transpolar arc. Figure 6a is drawn as the theta bar is entirely on closed field lines associated with sunward convection, although there is still room for the possibility that the dark region between the two transpolar arcs contains open field lines with antisunward flows [Burch et al., 1992]. After the B_Z spike a due northward MMF lasted for ~1.5 hours until 0022 UT. If we assume that the magnetosphere was in a steady state equilibrium, the sunward magnetic flux transport in the theta bar must be compensated by antisunward magnetic flux transport in the bifurcated polar cap. Namely, closed-to-open flux transfer at the high-latitude magnetopause and subsequent open-to-closed flux transfer in the magnetotail should occur, as explored by Kan and Burke [1985] and Reiff and Burch [1985].

After the southward turning of the MMF, reconnection between the southward MMF and the low-latitude closed geomagnetic field starts on the dayside, and antisunward flows are introduced from the dayside cusp into the polar cap (Figure 6b). The dawnside transpolar arc starts to decay shortly after the southward turning of the MMF and disappears within 10 min. The duskside transpolar arc, however, survives up until ~40 min after the southward turning of the MMF. Previous studies on the decay of polar cap arcs show that the timescale of the Sun-aligned arc disappearance associated with the southward turning of the IMF is the order of 15–20 min. Troshichev et al. [1988] investigated the response of polar cap arcs to a southward turning of the IMF in 17 events; they showed that in the 14 events of the 17, the time lag between the southward turning of the IMF and the polar cap arc disappearance fell within the 10–30 min range (the time resolution is 10 min). Rodriguez et al. [1997] examined six events of polar cap arc decay in which the decay was seemingly attributable to the dayside merging associated with a well-defined southward turning of the IMF; in their study the time lag between the southward turning of the IMF at the dayside magnetopause and the decay of the polar cap arcs ranged from 18 to 32 min. Thus the 40-min timescale determined in this study is not inconsistent with these previous studies, although it is a little longer than the typical values.

Now let us consider the 40-min persistence of the transpolar arc from a point of view of global ionospheric convection. After the southward turning of the MMF, dayside reconnection feeds antisunward flow in the dayside magnetosphere, and the flow tries to push back the expanded or bifurcated plasma sheet tailward. The plasma sheet, however, is filled with high-beta plasma and has a great deal of inertia. Namely, the theta bar behaves as an obstacle to the antisunward flow (Figure 6b). As a result, the antisunward flow is deflected toward the flanksides of the magnetosphere, and in the ionosphere the open magnetic flux added in the dayside cusp is preferably conveyed to the dawnside and duskside. During the 30 min following the southward turning of the MMF, the theta bar becomes thinner, and regions of open magnetic field lines grow in area on both sides of the theta bar, as inferred from the Søndre Strømfjord all-sky camera.

Forty minutes after the southward turning of the MMF, the theta bar at last starts to retreat antisunward (Figure 6c). This timescale is the same as that for the newly injected plasma associated with the dayside reconnection to proceed from the dayside cusp to the nightside polar cap boundary. We suspect, therefore, that the reconfiguration of the nightside plasma sheet is closely related to the mass and magnetic flux transport. The theta bar expands eastward and westward to conserve the magnetic flux. The distorted polar cap boundary on the nightside is gradually flattened out during the period of 0100–0120 UT. Thus the polar cap evolves into the normal circular shape. A substorm would have occurred if the southward MMF had continued.

Just before the extinction of the theta bar, however, an IMF $B_Z > 0$ pulse impinges on the magnetosphere, and the dayside reconnection rate reduces abruptly. As a consequence, the fast rarefaction wave is launched into the cusp/mantle region. At the same time the Alfvén wave is also emitted along the geomagnetic field lines onto the ionosphere. On reaching the cusp ionosphere the signal of the B_Z transition pervades the entire polar cap immediately (Figure 6d). This signal would be the fast rarefaction wave propagating across the magnetic field lines (although another candidate does exist, section 6.3). The B_Z signal is also transmitted to the nightside plasma sheet instantaneously. On the nightside the plasma sheet still holds a memory of the northward IMF period. That is, in a small region in or just above the northern ionosphere, a remnant of the sunward flow channel is still preserved in the expanded portion of the plasma sheet. Note that the sunward flow channel is suggested to have already been inactivated in the Southern Hemisphere. This north-south difference may arise from the effect of the sunlight, since the gradient of the plasma density, temperature, conductivity, etc. tends to be smoothed out in the sunlit hemisphere. When the B_Z transition signal reached the "fossil," a sunward flow burst is stimulated in the Northern Hemisphere. The electric field associated with the flow burst is then transmitted to the Southern Hemisphere along the magnetic field lines threading the outer boundary of the plasma sheet, and similar sunward flows are also observed in the southern ionosphere with a 7-min delay.

We should keep in mind here that the sunward flow in the Southern Hemisphere could be contributed to by the high-latitude reconnection associated with the northward IMF pulse. The dipole tilt angle and the positive IMF B_X sign during the pulse both favor open-to-open flux transfer at the high-latitude magnetopause in the Southern Hemisphere [e.g., Crooker, 1992]. The onset of the high-latitude reconnection would be retarded from the arrival of the B_Z transition at the

subsolar magnetopause. The DRV Y component in Figure 3 (the dayside cusp region) shows a positive excursion for 0136–0149 UT, which is nearly synchronized with the sunward flow in the Southern Hemisphere. This disturbance could be an ionospheric manifestation of the high-latitude reconnection that stimulates sunward convection. As we have seen, however, the morphology strongly suggests that the sunward flow bursts observed in both hemispheres are a geomagnetically conjugate phenomenon that originates in the same source region. Therefore we infer that the sunward flow bursts, at least their trigger, are attributable to the reduction of the reconnection rate at the subsolar magnetopause.

To summarize, two factors are responsible for the flow burst formation: (1) A remnant of the sunward flow channel had persisted up until the IMF jolt (internal condition), and (2) the IMF B_Z pulse reactivated the fossil of the sunward flow (external condition). Thus this phenomenon is a localized flow stimulation in the plasma sheet fragment trapped in the polar cap. Therefore it would not mean the change of the large-scale convection pattern in the entire polar region in response to the IMF B_Z pulse.

6.3. The Behavior of the Nightside Ionosphere-Magnetosphere System: Instantaneous or Retarded?

The ionospheric response time to changes in the IMF has been the subject of recent debate [*Lockwood and Cowley*, 1999; *Ridley et al.*, 1999]. The debate has focused on whether the convection pattern adjusts to the new IMF conditions by a near-instantaneous change in convection at all locations or whether the change originates in the dayside cusp and propagates away from this region.

In the event presented in this paper, there is no doubt that the electric field response is almost instantaneous and coherent over a wide region of the ionosphere, at least in the polar cap. The signal of the northward IMF B_Z transition did, in fact, reach the nightside ionosphere without a significant time delay (Figure 3), which is consistent with the work of *Ridley et al.* [1998] and *Ruohoniemi and Greenwald* [1998]. This indicates that the electric field disturbance in the dayside high-latitude ionosphere is communicated to the nightside ionosphere very quickly. The cause of this fast communication has not been identified yet. The most common idea would be the propagation of a fast mode MHD wave in the ionosphere. Another idea that has appeared in the literature is a transverse electromagnetic mode propagating with the speed of light in the insulating space between the conducting Earth and the conducting ionosphere [*Kikuchi and Araki*, 1979]. In either case the propagation is strongly affected by the inhomogeneity of ionospheric conductivities. In the latter model, the coupling mechanism between the magnetosphere and the Earth-ionosphere waveguide system is also a problem.

The change in convection may have been seen instantaneously throughout the polar cap, but it is not clear if the polar cap boundary has responded instantaneously (as sketched in Figure 3b of *Lockwood and Cowley* [1999] for a southward turning of the IMF). In other words, the question is whether the nightside polar cap boundary starts bulk motion on receiving the information from the dayside. Observationally, this has not been clarified in the past studies, possibly because of the difficulties in identifying the polar cap boundary. The motion of the nightside polar cap boundary depends on not only the dayside reconnection rate but also the nightside reconnection

rate. Here we assume that the nightside reconnection rate remains constant for a while (at least ~10 min) after the change of the dayside reconnection rate. In the event in this paper the polar cap boundary to the east of the Sun-aligned arc continued to move equatorward, even after the northward turning of the IMF, for more than 20 min (Plate 2; by 0155 UT the east-west arc marking the polar cap boundary left the field of view of the camera). Its overall equatorward motion looks rather smooth, and we cannot identify significant effects of the positive IMF B_Z pulse starting at 0128 UT. Namely, the equatorward speed of the polar cap boundary was ~0.2° min^{-1} both for 0123:47–0127:31 UT (Plates 2h–2j) and for 0129:23–0133:09 UT (Plates 2k–2m). (We tracked the point that gave the minimum magnetic latitude of the polar cap boundary.) This indicates that the potential change associated with the instantaneous ionospheric response has little or no effect on the polar cap boundary motion on the nightside, at least in this event.

We now need to consider how the immovable polar cap boundary and the coherent ionospheric response can coexist. One possible explanation to reconcile them would be that the potential change associated with the IMF transition is confined in the polar cap on the nightside at the early stage of the response. Namely, the equipotential contours do not cross the nightside polar cap boundary, or if they do, their effects on the nightside auroral oval (plasma sheet) are very small; that is, the magnitude of the flow change is too small to signify in the auroral oval. If we bear this picture in mind, the previously reported data are not inconsistent with this idea. For example, in the case of southward turnings of the IMF, Figure 8 of *Ridley et al.* [1998] shows almost no potential changes on the nightside; Figure 2 of *Ruohoniemi and Greenwald* [1998] shows a 2–4 min delay of the flow change onset at lower magnetic latitudes (73°–75°) in the dusk and premidnight sectors as compared to higher latitudes (note no SuperDARN observation at latitudes <73°). In the event in this paper we showed many examples of coherent magnetic field perturbations observed on the ground (Figure 3), but except for one station (DIX), they are all polar cap stations. We noted that the Greenland west coast magnetometer chain (not shown here) showed a qualitative change in the variations around the polar cap boundary. Although the coherent onsets of fluctuations were still discernible, the correlation to the MMF became somewhat obscure on the equatorward side of the polar cap boundary. Furthermore, the amplitude of the disturbance did not show an appreciable increase as expected from the increase of the Hall conductivity in the auroral oval. The latter implies the attenuation of the electric field in the plasma sheet. These facts may manifest the retarded response on the nightside.

Recently, *Lopez et al.* [1999], using MHD simulations, have proposed a similar explanation for the conflicting interpretations of previous studies. They suggest that the convection pattern across the entire polar cap changes immediately when the IMF goes southward but that the polar cap boundary expansion proceeds on a much longer timescale, with a delay of ~20 min between the dayside and the nightside. We should be careful, however, in interpreting their simulation results. Their results do show that the two-cell equipotential contours associated with the southward turning of the IMF cross the nightside polar cap boundary well before the onset of the equatorward motion of the nightside polar cap boundary. The resulting ionospheric flow at the nightside polar cap boundary is the order of 500–1000 m s^{-1} at F region altitudes. This is

inconsistent with the immovable polar cap boundary, since it is unthinkable that the nightside reconnection rate enhances immediately to such a high value in response to the ionospheric potential change in order to keep the polar cap boundary stationary. Thus, although Lopez et al.'s proposition is very suggestive, their simulation results are not straightforwardly convincing.

At this stage, the phenomenological character of the nightside response has not yet been clarified sufficiently to discuss and model the physics of the behavior of the nightside magnetosphere-ionosphere system. Here we point out some suggestions for the fast polar cap but retarded auroral oval response. We think the following two points are important: (1) how the large-scale static electric field is formed in the ionosphere and (2) how the magnetosphere reacts to the ionospheric electric field by Alfvénic coupling.

On the first point, whether the fast response of the ionosphere is carried by a fast mode MHD wave in the ionosphere or by an electromagnetic wave in the neutral atmosphere, it is not clear how these waves produce the large-scale static electric field that enhances or reduces the region 1/region 2 currents. To produce the static electric field, space charges must move in the opposite direction to the electric field. The difference in the efficiency or in the mechanism of the polarization may be a controlling factor of the fast polar cap but retarded auroral oval response.

The second point concerns the nature of magnetosphere-ionosphere coupling and, in particular, how the near-instantaneous ionospheric response to the imposed IMF conditions may require the ionosphere to drive the magnetosphere if a coupled system is to be maintained. In the region of closed magnetic field lines the region 1 and region 2 currents generated in the ionosphere must establish a closed circuit in the magnetospheric equator. The magnetospheric conductance (Σ_M) is considered to be smaller than the ionospheric Pedersen conductivity (Σ_P) [Nishida, 1978], and therefore the Alfvénic coupling of the ionosphere and the magnetosphere retards the ionospheric motion. If $\Sigma_M \ll \Sigma_P$, which is a reasonable assumption, the space charges generated in the ionosphere cannot be discharged in the magnetosphere via field-aligned currents. Instead, they are dissipated in the ionosphere, resulting in the cancellation of the electric field. This means that the ionosphere feels self-force, and its motion is retarded. In contrast, the region of open magnetic field lines is not subjected to the magnetospheric feedback, because the current circuit does not need to be closed. This may be the cause of the different behavior of the polar cap and the auroral oval. It is noted, however, that the feedback on the ionosphere starts on a timescale for the Alfvén wave to travel back and forth between the ionosphere and the magnetosphere. In the event in this paper we interpreted the 7-min time lag of the flow burst onset between the northern and southern ionospheres as the Alfvén travel time along the field lines. According to the above scenario, the magnetospheric feedback should commence ~7 min after the first ionospheric response. This is not supported by the observation, since the retarding seems to take effect without significant delay. There may be some mechanisms that shorten the timescale of the magnetosphere-ionosphere coupling, or the above scenario may not be the case.

The above discussion is far from complete and needs further investigation in future studies. In concluding, we emphasize the following. There is no doubt that the ionospheric response to an IMF change is very fast and that the polar ionosphere seems able to respond to the solar wind conditions faster than the magnetosphere. This urges us to reconsider the role of the ionosphere in magnetospheric physics. The ionosphere is not merely a passive dissipater but can be an active driver.

7. Conclusions

We have found observational evidence for a rapid communication of IMF changes to the global ionosphere and evidence for the state of the magnetosphere in the previous hour conditioning this response. These conclusions are drawn from a case study of sunward flow bursts on the nightside polar cap boundary observed by geomagnetically conjugate HF radars. The flow burst excitation consists of two factors: (1) A remnant of the sunward flow channel that had persisted previously (i.e., a "fossil" of the theta aurora) was still preserved in the poleward expanded portion of the plasma sheet (internal condition), and (2) an IMF transition from southward to northward B_Z impinged on the magnetosphere and reactivated the sunward flow channel (external condition). This nightside phenomenon represents a rapid global response of the ionosphere starting 2–3 min after the IMF transition at the subsolar magnetopause.

Appendix: Instrumentation and Data Display

The Goose Bay radar observes a large volume of the ionosphere above Greenland and northeastern Canada, whereas the Halley radar observes the geomagnetically conjugate region of the Goose Bay radar field of view in the Antarctic ionosphere. See Table 1 for the radar locations. The Goose Bay radar scans over a 52° azimuth sector centered on 5° east of geographic north (11° east of geomagnetic north). Similarly, the Halley radar scans over a 52° azimuth sector centered on 15° east of geographic south (geomagnetic meridian). See Figure 1 for the fields of view. Both radars scan over the azimuthal sector in 16 beam steps. They operate at frequencies between 8 and 20 MHz and measure the coherent backscattered power and Doppler spectral characteristics of decameter-range field-aligned irregularities in the E and F regions. For details about the radars' operational characteristics, see the work of Greenwald et al. [1995]. During the period of our interest, the azimuthal scanning was performed every 100 s, and the backscatter was range-gated in steps of 45 km for both radars. At F region altitudes the line-of-sight Doppler velocity of the irregularities gives a measure of the electric field drift of the plasma. Plates 1 and 3 show the line-of-sight Doppler velocities observed by the Goose Bay and Halley HF radars, respectively. Both are plotted in the AACGM coordinate system. Here we assumed that all the F region echoes were scattered from an altitude of 400 km.

Eureka is located near the geomagnetic North Pole and suitable for the observation of polar cap arcs. The all-sky camera at Eureka is equipped with 558- and 630-nm filters and was operated in a time-lapse mode with a three-frame sequence of broadband (unfiltered), green line (558 nm), and red line (630 nm) emissions recorded each 8 s. See Figure 1a for the field of view. Plate 5 shows selected images of the green line emission recorded with a 1/32 s integration. At Eureka a three-component flux gate magnetometer is also operated continuously. The dot outside the rim in Plate 5 denotes the direction of the D component presented in Figure 3.

Søndre Strømfjord on the west coast of Greenland lies within the field of view of the Goose Bay radar. It is a place where many ground-based remote-sensing instruments are assembled for upper atmosphere research [Kelly et al., 1995]. In this paper we utilized data from the all-sky camera and the incoherent scatter radar. The all-sky camera is equipped with five filters with an angular resolution of ~0.5°. See Figure 1a for the field of view. During the period of interest, the operation program of the camera cycled through four filters (428, 630, 486, and 490 nm) in 114 s. Plate 2 illustrates selected images of the 630-nm emission recorded with an exposure duration of 9 s.

The incoherent scatter radar at Søndre Strømfjord (the Sondrestrom IS radar) operates at frequencies 1.28–1.30 GHz and measures the electron density, line-of-sight ion velocity, and electron and ion temperatures (see Kelly et al. [1995] for details). During the period of interest, the radar was performing elevation scans and three-fixed-position scans alternatively. The elevation scan was performed in the plane near to the geomagnetic meridian shown in Figure 1a by the thick line passing through the radar site (STF). In this paper we present ion drift velocities in the geomagnetic meridional plane derived from the line-of-sight velocities during the elevation scans. Generally, field-aligned ion velocities are much smaller than field-perpendicular velocities in the F region, so we assumed that the line-of-sight velocity (V_{los}) obtained by the IS radar was the line-of-sight component of the field-perpendicular velocity ($V_\perp$), namely, $V_\perp = V_{los}/\sin(\theta)$, where θ is the angle sustained by the geomagnetic field and the wave normal. Figure 5 shows the ion drift velocities averaged in the MLAT bins. The data at altitudes >180 km were first calibrated to the values at 300-km altitude using a dipole magnetic field. After the exclusion of unreliable data ($|V_\perp| > 2000$ m s^{-1}, $V_{\perp error} > 250$ m s^{-1}), three quartiles (the median and the upper and lower quartiles) were determined in each MLAT bin. The velocities thus determined are interpreted to represent the geomagnetic north-south component of the cross-field ion drifts (positive northward).

The DMSP satellites carry electrostatic analyzers (SSJ4) designed to measure the flux of precipitating electrons and ions in the energy range 0.03–30 keV in 19 logarithmically spaced steps [Hardy et al., 1984]. They also carry a thermal plasma detector (SSIES), which includes an ion drift meter to measure the plasma flow velocities perpendicular to the satellite's track [Greenspan et al., 1986]. The NOAA 12 spacecraft instrument includes electrostatic analyzers (TED) to measure the integrated directional energy flux carried into the atmosphere by electrons and ions in the energy range 0.3–20 keV at two pitch angles [Hill et al., 1985]. We utilized precipitating particle or cross-track ion drift data obtained by these satellites wherever possible. Figure 4 illustrates a concise summary of the observations. Plate 4 shows one particular overflight of F11 in the field of view of the Halley radar.

References

Banks, P. M., C. R. Chappell, and A. F. Nagy, A new model for the interaction of auroral electrons with the atmosphere: Spectral degradation, backscatter, optical emission, and ionization, J. Geophys. Res., 79, 1459–1470, 1974.

Bhavnani, K. H., and C. A. Hein, An improved algorithm for computing altitude dependent corrected geomagnetic coordinates, Tech. Rep. PL-TR-94-2310, Phillips Lab., Hanscom Air Force Base, Bedford, Mass., 1994.

Blanchard, G. T., L. R. Lyons, and J. C. Samson, Accuracy of using 6300 Å auroral emission to identify the magnetic separatrix on the nightside of Earth, J. Geophys. Res., 102, 9697–9703, 1997.

Burch, J. L., N. A. Saflekos, D. A. Gurnett, J. D. Craven, and L. A. Frank, The quiet time polar cap: DE1 observations and conceptual model, J. Geophys. Res., 97, 19,403–19,412, 1992.

Bythrow, P. F., W. J. Burke, T. A. Potemra, L. J. Zanetti, and A. T. Y. Lui, Ionospheric evidence for irregular reconnection and turbulent plasma flows in the magnetotail during periods of northward interplanetary magnetic field, J. Geophys Res., 90, 5319–5325, 1985.

Carlson, H. C., R. A. Heelis, E. J. Weber, and J. R. Sharber, Coherent mesoscale convection patterns during northward interplanetary magnetic field, J. Geophys. Res., 93, 14,501–14,514, 1988.

Chang, S.-W., et al., A comparison of a model for the theta aurora with observations from Polar, Wind, and SuperDARN, J. Geophys. Res., 103, 17,367–17,390, 1998.

Clauer, C. R., and E. Friis-Christensen, High-latitude dayside electric fields and currents during strong northward interplanetary magnetic field: Observations and model simulations, J. Geophys. Res., 93, 2749–2757, 1988.

Cowley, S. W. H., and M. Lockwood, Excitation and decay of solar wind-driven flows in the magnetosphere-ionosphere system, Ann. Geophys., 10, 103–115, 1992.

Crooker, N. U., Reverse convection, J. Geophys. Res., 97, 19,363–19,372, 1992.

Cumnock, J. A., J. R. Sharber, R. A. Heelis, M. R. Hairston, and J. D. Craven, Evolution of the global aurora during positive IMF B_z and varying IMF B_Y conditions, J. Geophys. Res., 102, 17,489–17,497, 1997.

Etemadi, A., S. W. H. Cowley, M. Lockwood, B. J. I. Bromage, D. M. Willis, and H. Lühr, The dependence of high-latitude dayside ionospheric flows on the north-south component of the IMF: A high time resolution correlation analysis using EISCAT "Polar" and AMPTE UKS and IRM data, Planet. Space Sci., 36, 471–498, 1988.

Frank, L. A., et al., The theta aurora, J. Geophys. Res., 91, 3177–3224, 1986.

Freeman, M. P., J. M. Ruohoniemi, and R. A. Greenwald, The determination of time-stationary two-dimensional convection patterns with single-station radars, J. Geophys. Res., 96, 15,735–15,749, 1991.

Greenspan, M. E., P. B. Anderson, and J. M. Pelagatti, Characteristics of the thermal plasma monitor (SSIES) for the Defense Meteorological Satellite Program (DMSP) spacecraft F8 through F10, *Tech. Rep. AFGL-TR-86-0227*, Air Force Geophys. Lab., Hanscom Air Force Base, Bedford, Mass., 1986.

Greenwald, R. A., et al., DARN/SuperDARN: A global view of the dynamics of high-latitude convection, *Space Sci. Rev.*, *71*, 761–796, 1995.

Hairston, M. R., and R. A. Heelis, Response time of the polar cap ionospheric convection pattern to changes in the north-south direction of the IMF, *Geophys. Res. Lett.*, *22*, 631–634, 1995.

Hardy, D. A., L. K. Schmidtt, M. S. Gussenhoven, F. J. Marshall, H. C. Yeh, T. L. Shumaker, A. Hube, and J. Pantazis, Precipitating electron and ion detectors (SSJ/4) for the block 5D/flights 6–10 DMSP satellites: Calibration and data presentation, *Tech. Rep. AFGL-TR-84-0317*, Air Force Geophys. Lab., Hanscom Air Force Base, Bedford, Mass., 1984.

Heppner, J. P., and N. C. Maynard, Empirical high-latitude electric field models, *J. Geophys. Res.*, *92*, 4467–4489, 1987.

Hill, V. J., D. S. Evans, and H. H. Sauer, TIROS/NOAA satellites space environment monitor archive tape documentation, *NOAA Tech. Memo. ERL SEL-71*, Space Environ. Lab., Boulder, Colo., 1985.

Kan, J. R., and W. J. Burke, A theoretical model of polar cap auroral arcs, *J. Geophys. Res.*, *90*, 4171–4177, 1985.

Kelly, J. D., C. J. Heinselman, J. F. Vickrey, and R. R. Vondrak, The Sondrestrom radar and accompanying ground-based instrumentation, *Space Sci. Rev.*, *71*, 797–813, 1995.

Kikuchi, T., and T. Araki, Horizontal transmission of the polar electric field to the equator, *J. Atmos. Terr. Phys.*, *41*, 927–936, 1979.

Knipp, D. J., A. D. Richmond, B. Emery, N. U. Crooker, O. de la Beaujardière, D. Evans, and H. Kroehl, Ionospheric convection response to changing IMF direction, *Geophys. Res. Lett.*, *18*, 721–724, 1991.

Lockwood, M., and S. W. H. Cowley, Comment on "A statistical study of the ionospheric convection response to changing interplanetary magnetic field conditions using the assimilative mapping of ionospheric electrodynamics technique" by A. J. Ridley et al., *J. Geophys. Res.*, *104*, 4387–4391, 1999.

Lockwood, M., A. P. van Eyken, B. J. I. Bromage, D. M. Willis, and S. W. H. Cowley, Eastward propagation of a plasma convection enhancement following a southward turning of the interplanetary magnetic field, *Geophys. Res. Lett.*, *13*, 72–75, 1986.

Lopez, R. E., M. Wiltberger, J. G. Lyon, C. C. Goodrich, and K. Papadopoulos, MHD simulations of the response of high-latitude potential patterns and polar cap boundaries to sudden southward turnings of the interplanetary magnetic field, *Geophys. Res. Lett.*, *26*, 967–970, 1999.

Morelli, J. P., et al., Radar observations of auroral zone flows during a multiple-onset substorm, *Ann. Geophys.*, *13*, 1144–1163, 1995.

Newell, P. T., and C.-I. Meng, Creation of theta-auroras: The isolation of plasma sheet fragments in the polar cap, *Science*, *270*, 1338–1341, 1995.

Nishida, A., Coherence of geomagnetic *DP* 2 fluctuations with interplanetary magnetic variations, *J. Geophys. Res.*, *73*, 5549–5559, 1968.

Nishida, A., *Geomagnetic Diagnosis of the Magnetosphere*, chap. 3.5, Springer-Verlag, New York, 1978.

Phan, T.-D., G. Paschmann, W. Baumjohann, N. Sckopke, and H. Lühr, The magnetosheath region adjacent to the dayside magnetopause: AMPTE/IRM observations, *J. Geophys. Res.*, *99*, 121–141, 1994.

Reiff, P. H., and J. L. Burch, IMF B_Y-dependent plasma flow and Birkeland currents in the dayside magnetosphere, 2, A global model for northward and southward IMF, *J. Geophys. Res.*, *90*, 1595–1609, 1985.

Ridley, A. J., G. Lu, C. R. Clauer, and V. O. Papitashvili, Ionospheric

convection during nonsteady interplanetary magnetic field conditions, *J. Geophys. Res.*, *102*, 14,563–14,579, 1997.

Ridley, A. J., G. Lu, C. R. Clauer, and V. O. Papitashvili, A statistical study of the ionospheric convection response to changing interplanetary magnetic field conditions using the assimilative mapping of ionospheric electrodynamics technique. *J. Geophys. Res.*, *103*, 4023–4039, 1998.

Ridley, A. J., G. Lu. C. R. Clauer, and V. O. Papitashvili, Reply, *J. Geophys. Res.*, *104*, 4393–4396, 1999.

Rodriguez, J. V., C. E. Valladares, K. Fukui, and H. A. Gallagher Jr., Antisunward decay of polar cap arcs, *J. Geophys. Res.*, *102*, 27,227–27,247, 1997.

Ruohoniemi, J. M., and R. A. Greenwald, The response of high-latitude convection to a sudden southward IMF turning, *Geophys. Res. Lett.*, *25*, 2913–2916, 1998.

Saunders, M. A., M. P. Freeman, D. J. Southwood, S. W. H. Cowley, M. Lockwood, J. C. Samson, C. J. Farrugia, and T. J. Hughes, Dayside ionospheric convection changes in response to long-period interplanetary magnetic field oscillations: Determination of the ionospheric phase velocity, *J. Geophys. Res.*, *97*, 19,373–19,380, 1992.

Spreiter, J. R., and S. S. Stahara, A new predictive model for determining solar wind-terrestrial planet interaction, *J. Geophys. Res.*, *85*, 6769–6777, 1980.

Taylor, J. R., S. W. H. Cowley, T. K. Yoeman, M. Lester, T. B. Jones, R. A. Greenwald, G. Sofko, J.-P. Villain, R. P. Lepping, and M. R. Hairston, SuperDARN studies of the ionospheric convection response to a northward turning of the interplanetary magnetic field, *Ann. Geophys.*, *16*, 549–565, 1998.

Thayer, J. P., G. Crowley, R. J. Niciejewski, T. L. Killeen, J. Buchau, and B. W. Reinisch, Ground-based observations of ion/neutral coupling at Thule and Qânâq, Greenland, *J. Geophys. Res.*, *100*, 12,189–12,199, 1995.

Todd, H., S. W. H. Cowley, M. Lockwood, D. M. Willis, and H. Lühr, Response time of the high-latitude dayside ionosphere to sudden changes in the north-south component of the IMF, *Planet. Space Sci.*, *36*, 1415–1428, 1988.

Troshichev, O. A., M. G. Gusev, S. V. Nickolashkin, and V. P. Samsonov, Features of the polar cap aurorae in the southern polar region, *Planet. Space Sci.*, *36*, 429–439, 1988.

Watanabe, M., M. Pinnock, A. S. Rodger, N. Sato, H. Yamagishi, A. S. Yukimatu, R. A. Greenwald, J.-P. Villain, and M. R. Hairston, Localized activation of the distant tail neutral line just prior to substorm onsets, *J. Geophys. Res.*, *103*, 17,651–17,669, 1998.

R. A. Greenwald, Applied Physics Laboratory, Johns Hopkins University, Johns Hopkins Road, Laurel, MD 20723-6099. (ray_greenwald@jhuapl.edu)

M. R. Hairston, William B. Hanson Center for Space Sciences, University of Texas at Dallas, P.O. Box 830688 F022, Richardson, TX 75083-0688. (hairston@utdallas.edu)

D. J. McEwen, Department of Physics and Engineering Physics, College of Arts and Science, University of Saskatchewan, 116 Science Place, Saskatoon, Saskatchewan, Canada S7N 5E2. (mcewen@skisas.usask.ca)

M. Pinnock, British Antarctic Survey, Natural Environment Research Council, High Cross, Madingley Road, Cambridge CB3 0ET, England, U.K. (M.Pinnock@bas.ac.uk)

R. L. Rairden, Space Sciences Laboratory, Lockheed Missiles and Space Company, Inc., 3251 Hanover Street, Palo Alto, CA 94304-1191. (rairden@agena.spasci.com)

N. Sato and M. Watanabe, National Institute of Polar Research, 1-9-10 Kaga, Itabashi, Tokyo 173-8515, Japan. (nsato@nipr.ac.jp; maskaz@nipr.ac.jp)